Cerveau Humain $>10^{10}$x

Vue latérale hémisphère gauche

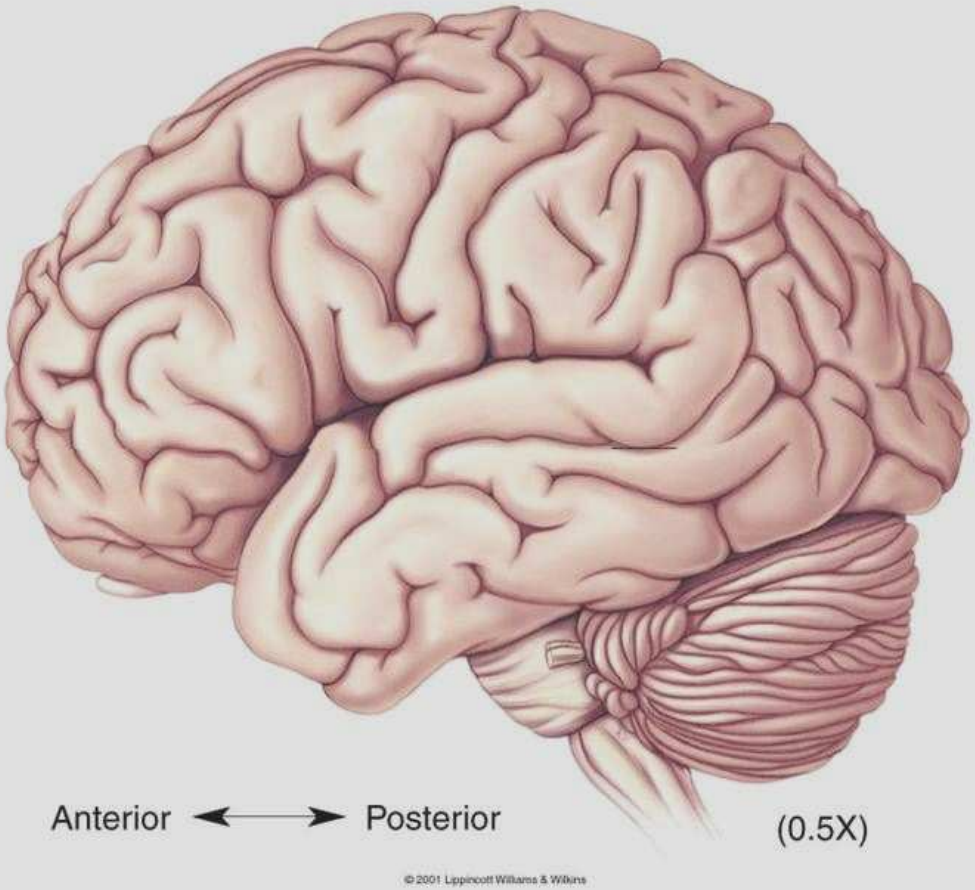

Neurone(s)

Cellule pyramidale de la couche 6 du cortex visuel primaire

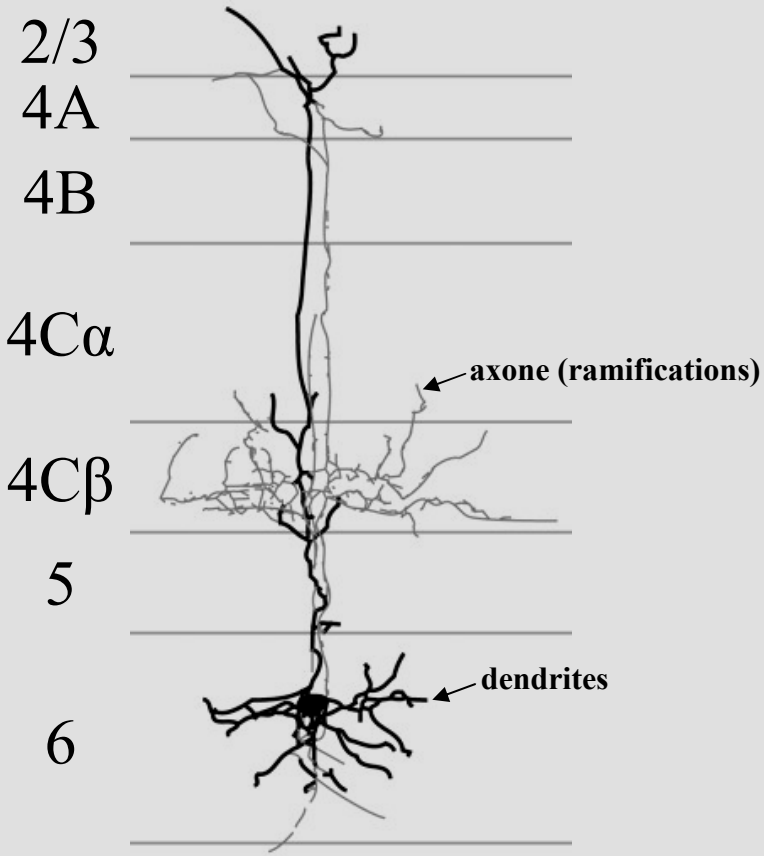

F. Briggs and E. M. Callaway, J.o.N.S., ´01

Reference

- La vision, mission du cerveau

  Guy Orban

- College de France/Fayard 2007

  (serie des lecons inaugurales du college de France)

Strategies de recherche

Les niveaux d'intégration dans le cerveau

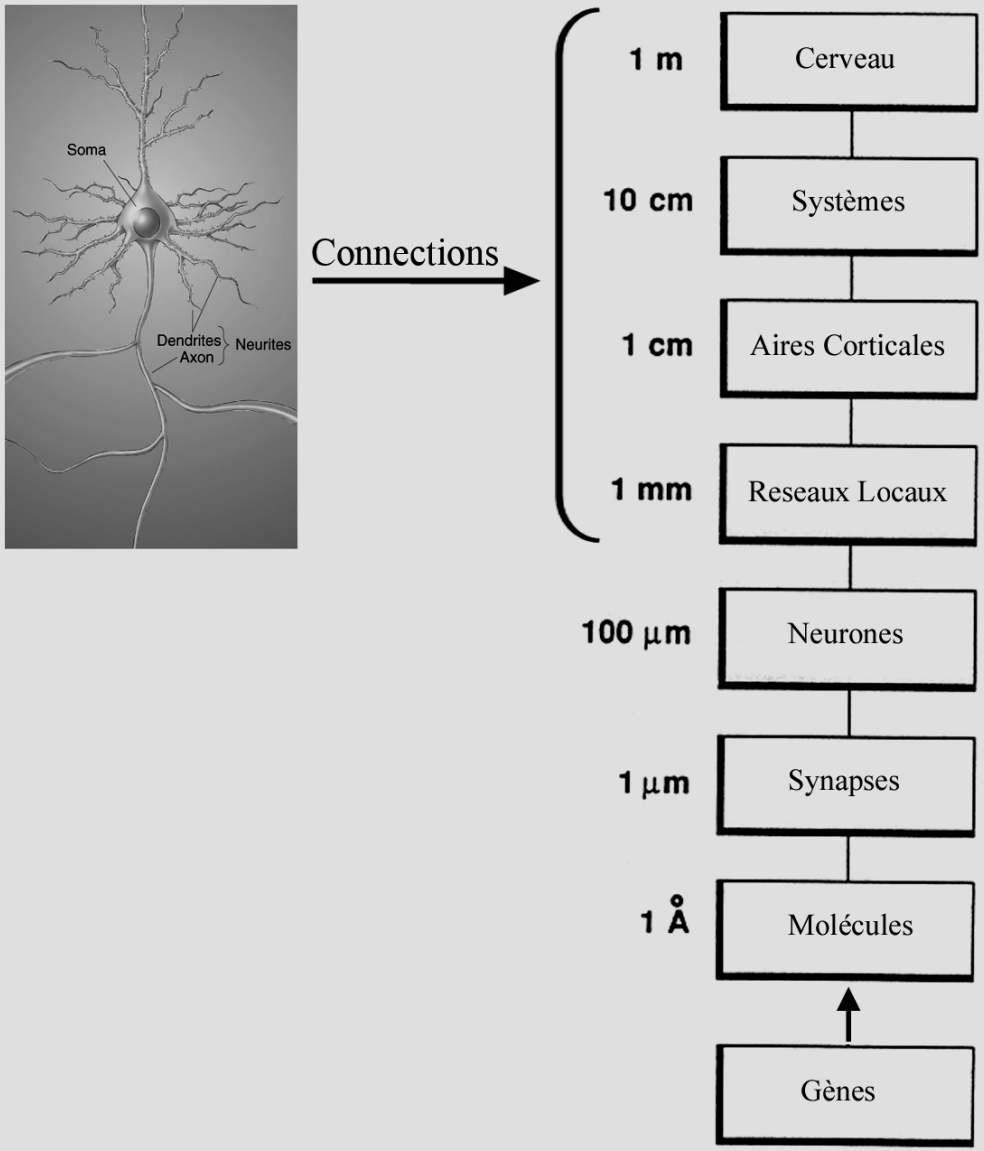

Les techniques expérimentales

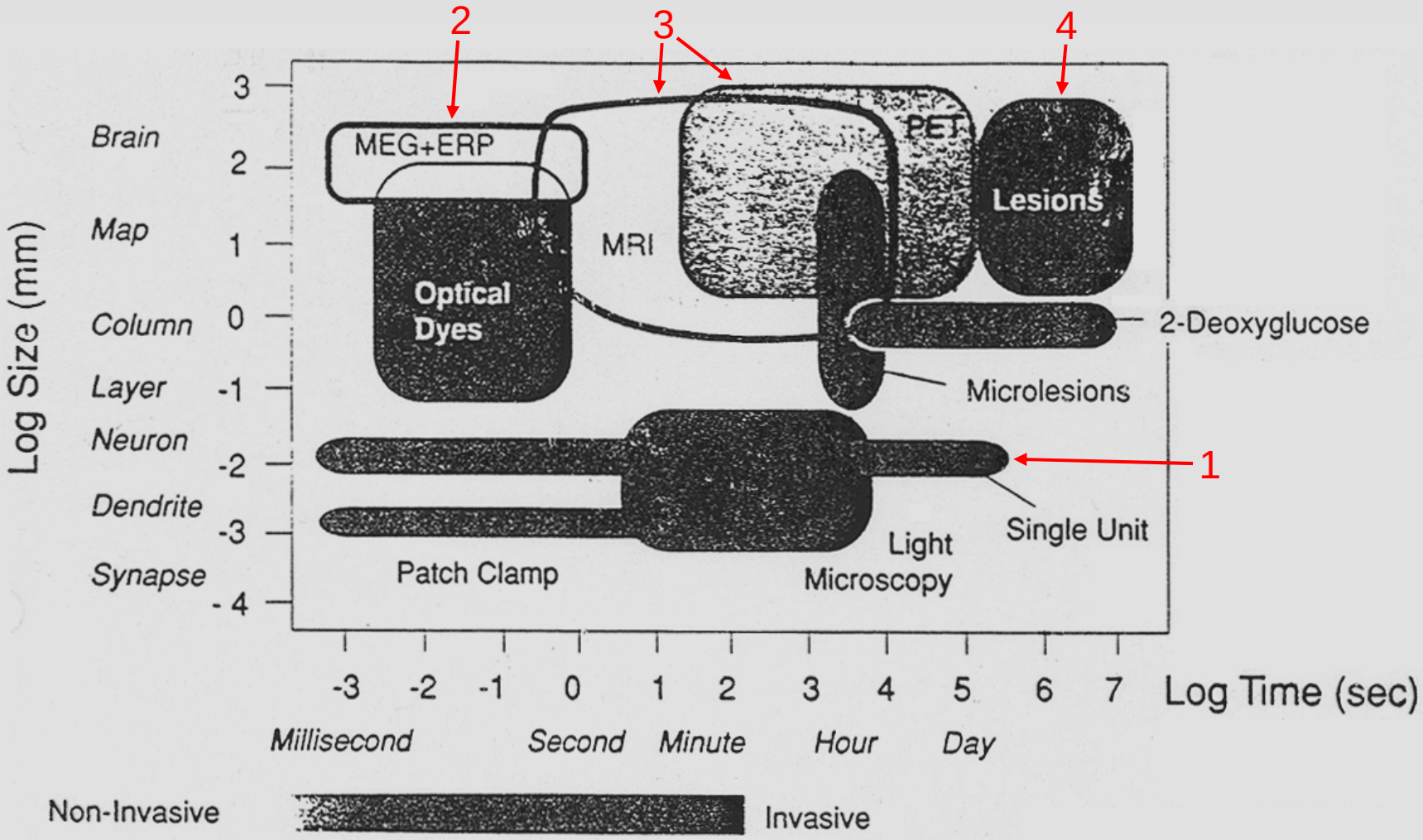

MEG - magnetoencephalography; *ERP* - evoked response potential (EEG); *PET* - positron emission tomography; *2-Deoxyglucose* - autoradiography; *MRI* - magnetic resonance

La triade des neurosciences cognitives

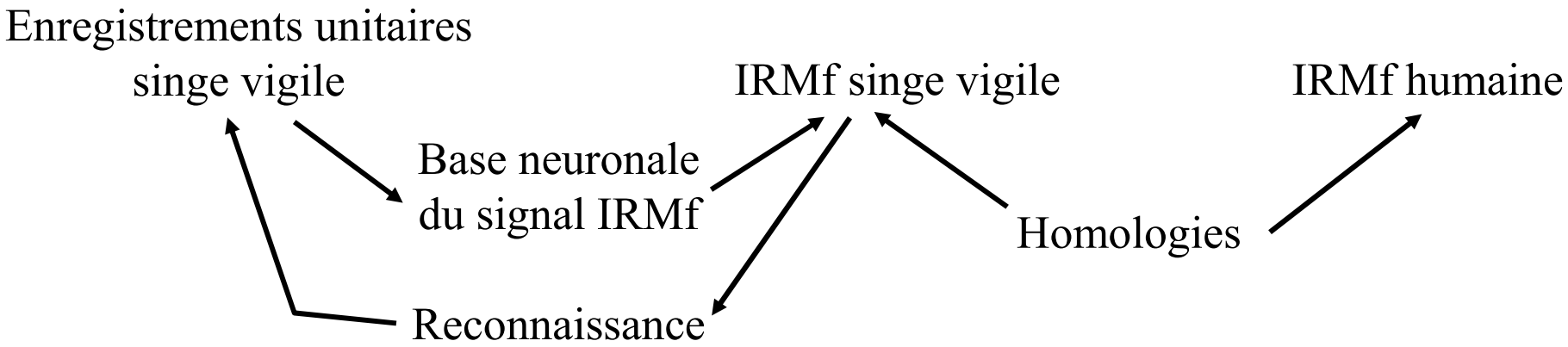

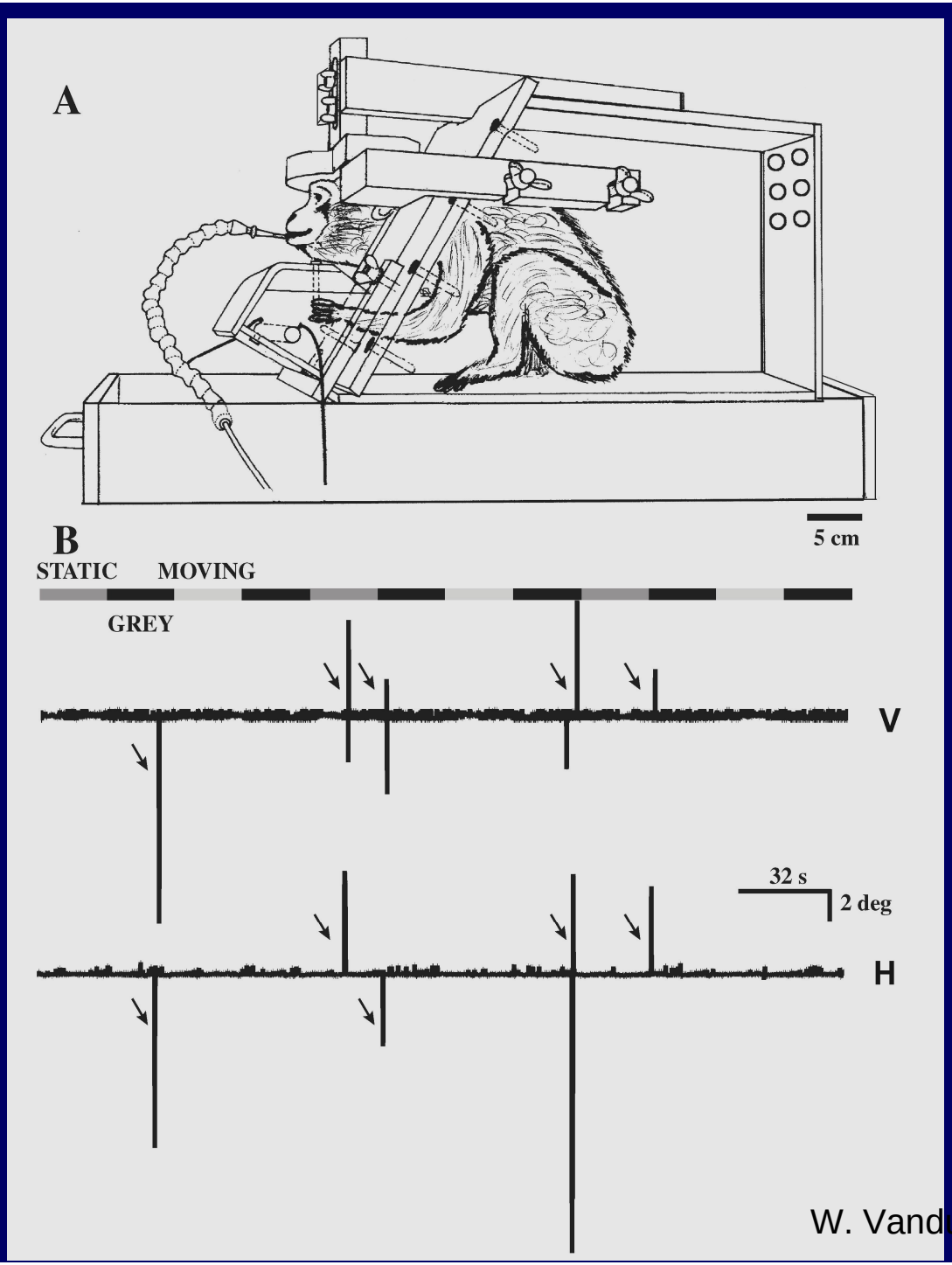

W. Vanduffel et al, Neuron, '01

CHAMP RECEPTEUR

Definition

- Propriete d’un neurone
- Partie de la surface de reception (peau, retine)
- Partie de cete surface innervee par le neurone, donc la partie dont la stimulation active le neurone

CHAMP RECEPTEUR (CR)

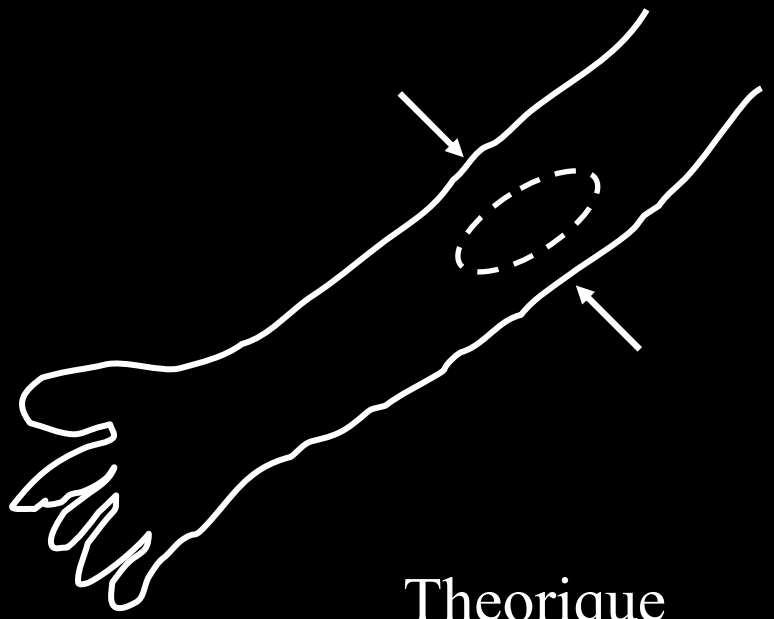

Theorique

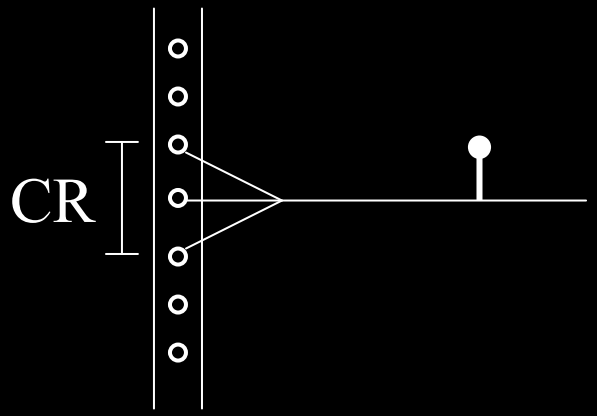

Pratique

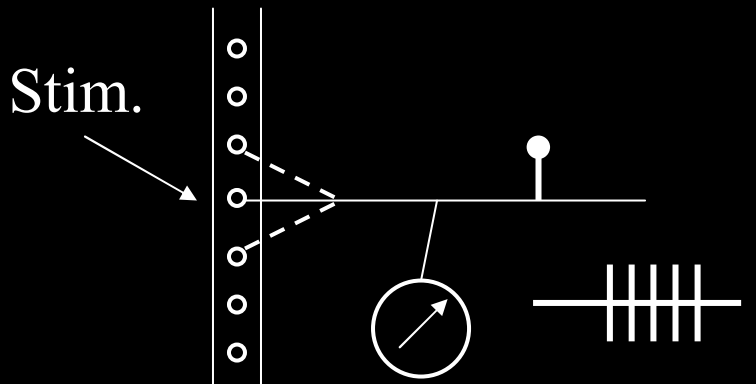

DENSITE d' INNERVATION

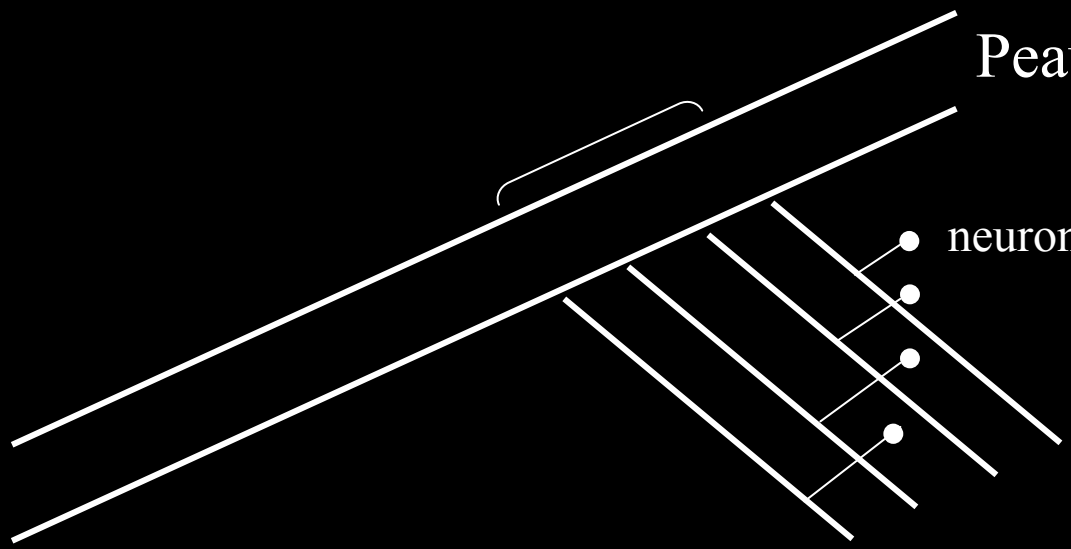

nb neurones / unite surface

Grande

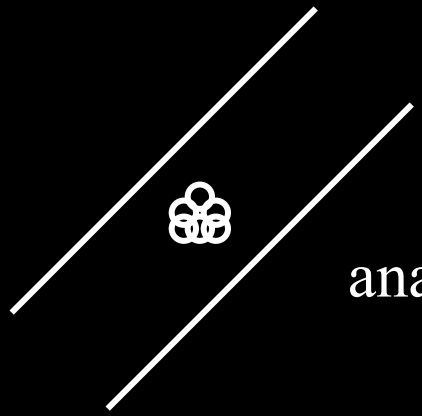

analyse

Petite

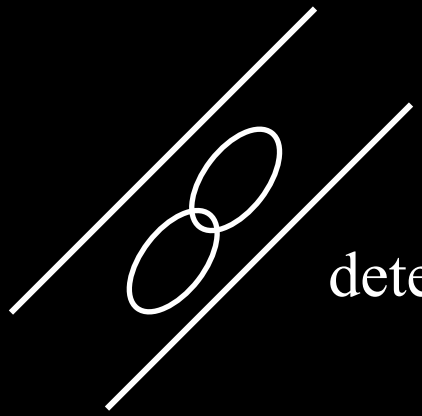

detection

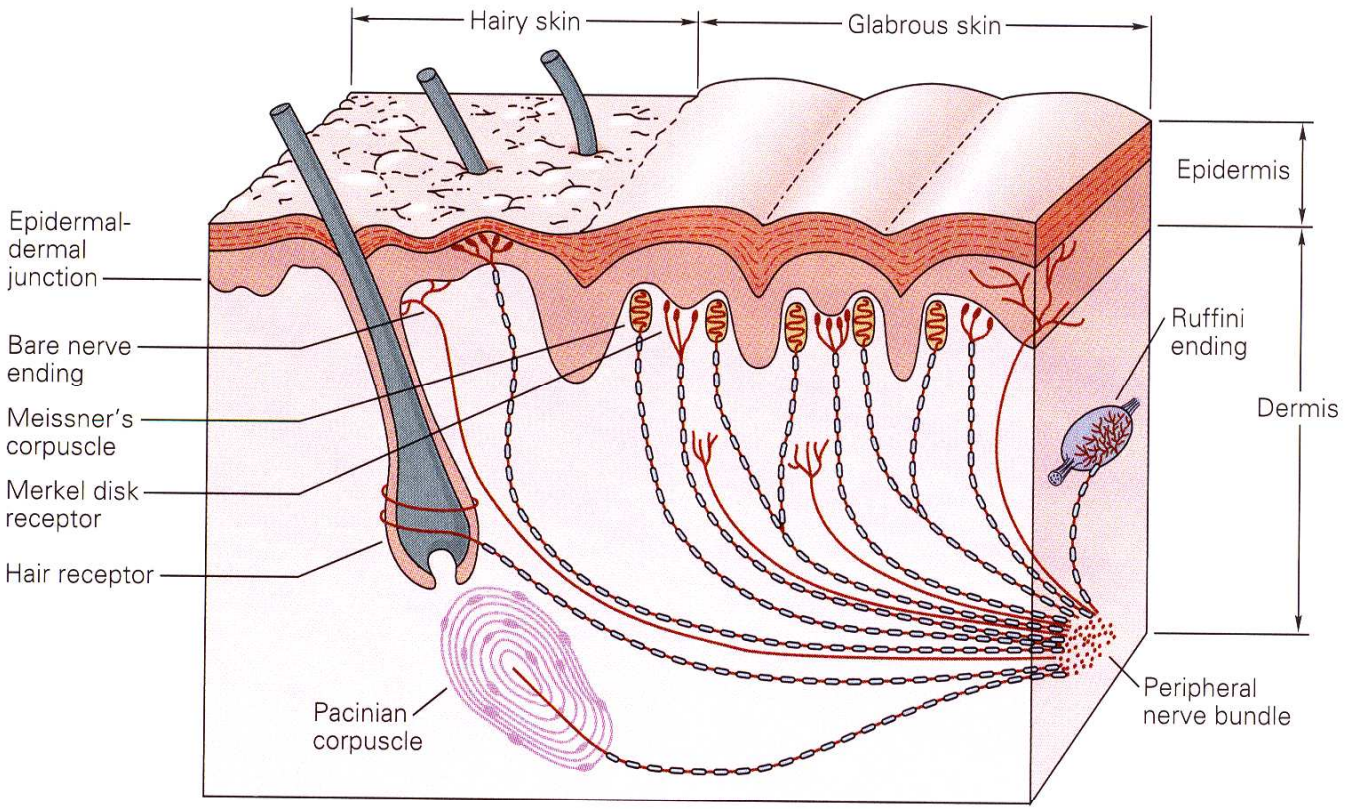

Figure 22-2 The location and morphology of mechanoreceptors in hairy and hairless (glabrous) skin of the human hand. Receptors are located in the superficial skin, at the junction of the dermis and epidermis, and more deeply in the dermis and subcutaneous tissue. The receptors of the glabrous skin are Meissner's corpuscles, located in the dermal papillae; Merkel disk receptors, located between the dermal papillae; and bare nerve endings. The receptors of the hairy skin are hair receptors, Merkel's receptors (having a slightly different organization than their counterparts in the glabrous skin), and bare nerve endings. Subcutaneous receptors, beneath both glabrous and hairy skin, include Pacinian corpuscles and Ruffini endings. Nerve fibers that terminate in the superficial layers of the skin are branched at their distal terminals, innervating several nearby receptor organs; nerve fibers in the subcutaneous layer innervate only a single receptor organ. The structure of the receptor organ determines its physiological function.

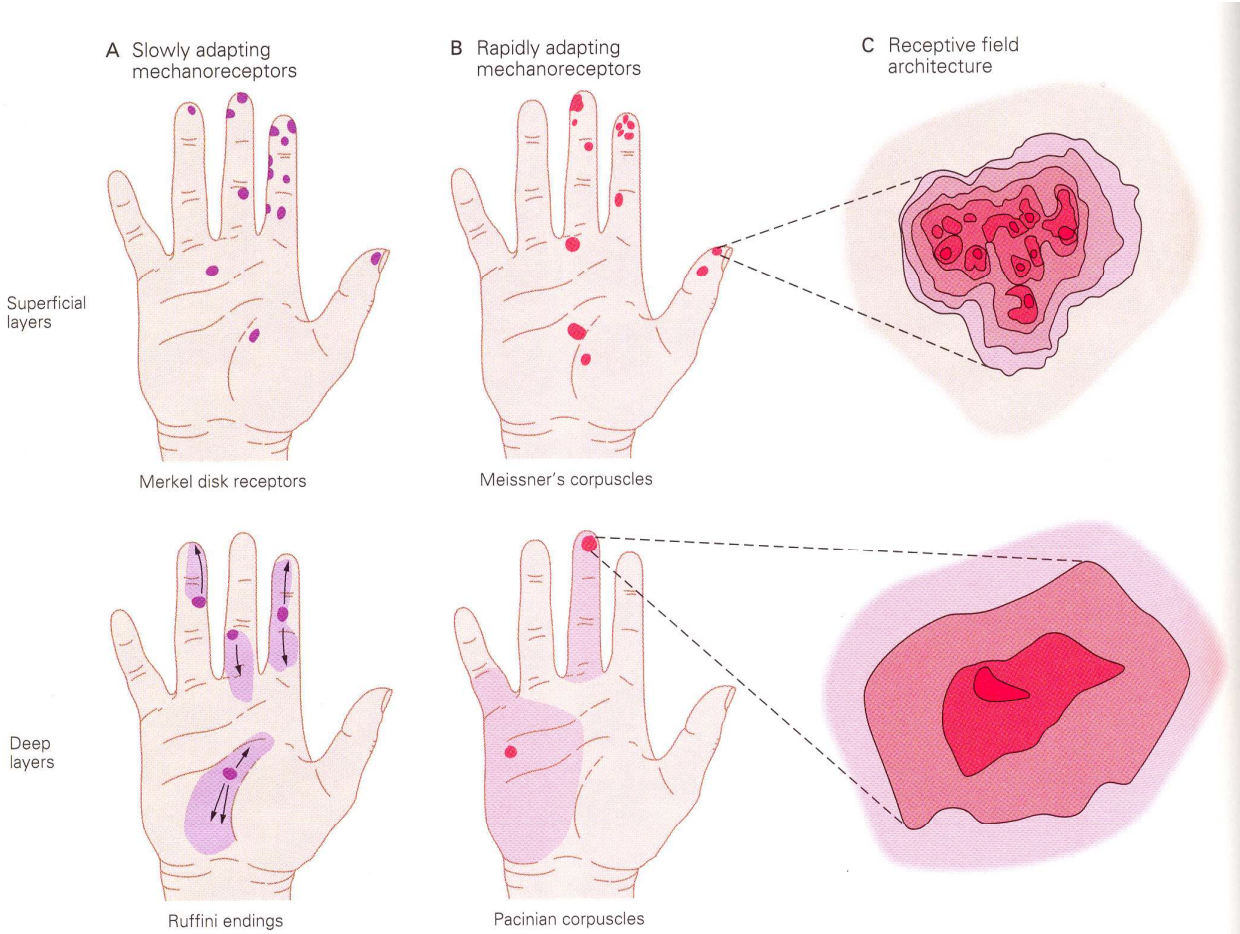

Figure 22-3 Mechanoreceptors in glabrous skin vary in the size and structure of their receptive fields. Each colored area on the hands indicates the receptive field of a different sensory nerve fiber in the human median nerve. (Adapted from Johansson and Vallbo 1983.)

A. The Merkel disk receptor in the superficial skin and the subcutaneous Ruffini ending are slowly adapting receptors (see Figure 21-9A). The Merkel disk receptor has a small, highly localized receptive field, whereas the Ruffini ending has a large field (**light purple**) with a central zone of maximal sensitivity (**dark purple**). Depending on their location, individual Ruffini endings are excited by stretch of the skin in specific directions as indicated by arrows.

B. The Meissner's corpuscle in the superficial skin and the subcutaneous Pacinian corpuscle are rapidly adapting receptors (see Figure 21-9B). Meissner's corpuscles on the fingertips have receptive fields averaging 2–3 mm in diameter, while receptive fields on the palm average 10 mm in diameter. The receptive fields of Pacinian corpuscles cover larger continuous surfaces on the fingers or palm (**light pink**) but have a central zone of maximal sensitivity located directly above the receptor (**red**).

C. Expanded view of the receptive fields of mechanoreceptors in the superficial and deep layers of glabrous skin. The relative sensitivity to pressure is shown as a contour map in which the most sensitive regions are indicated in **red** and the least sensitive areas in **pale pink.** Receptive fields in the superficial layers of the skin have many points of high sensitivity, marking the positions of the Meissner's corpuscles or Merkel disk receptors. Receptive fields in the deep layers have a single point of maximal sensitivity overlying the Pacinian or Ruffini receptor.

Figure 23-10 The receptive field of a higher-order neuron in the dorsal column nuclei has a characteristic pattern of excitation and inhibition that increases spatial resolution.

A. Many peripheral receptors converge onto a single second-order sensory neuron in the dorsal column nuclei. As a consequence, the excitatory receptive field of the central neuron is made up of the receptive fields of all the presynaptic cells.

B. The receptive field of a neuron in the dorsal column nuclei and in the ventral posterior nuclei of the thalamus typically has a central excitatory receptive field surrounded or flanked by an inhibitory region. The addition of inhibitory interneurons (**gray**) narrows the discharge zone. Feed-forward inhibition sharpens the representation of a punctate stimulus by limiting the spread of excitation through convergent neural networks. On either side of the excitatory region the discharge rate is driven below the resting level by inhibition.

C. The asymmetric distribution of inhibitory interneurons produces lateral inhibition. In this schematic network, stimulation in the upper portion of the receptive field produces strong excitation of the relay neuron. Stimulation of the lower portion of the receptive field inhibits firing because the interneurons produce feed-forward inhibition. Stimulation in the zone of overlap of excitation and inhibition reduces the responsiveness of the relay neuron to the stimulus. Lateral inhibition is particularly important for feature detection.

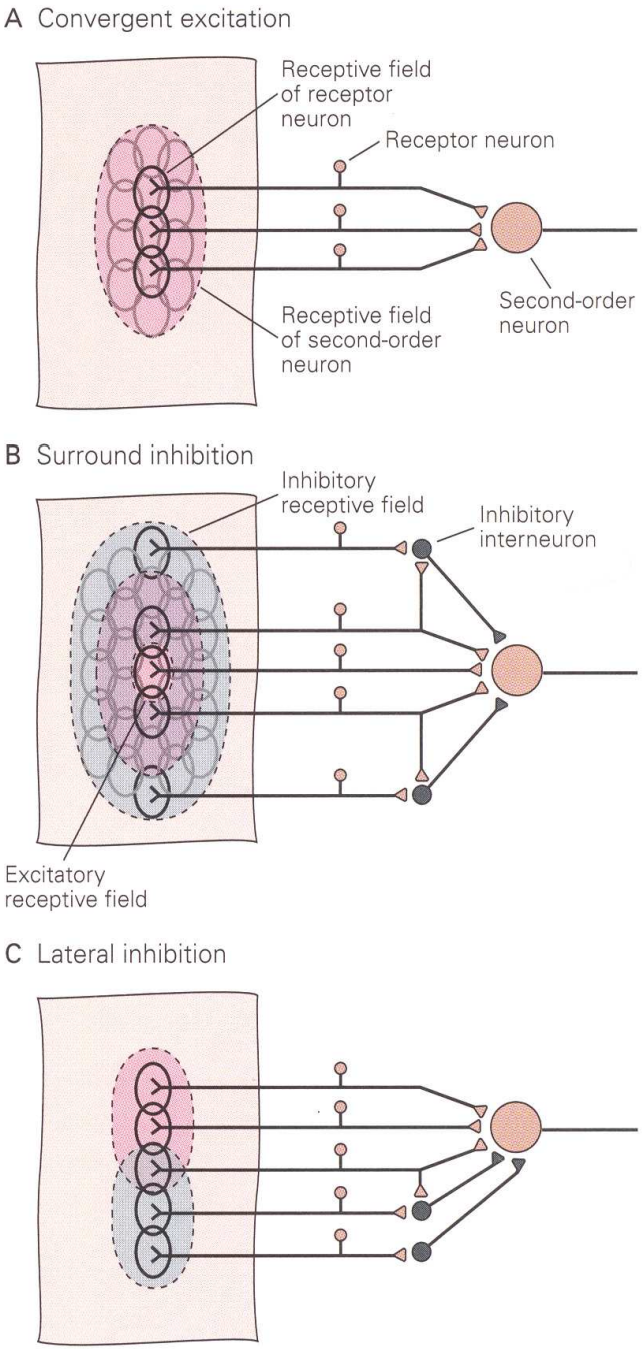

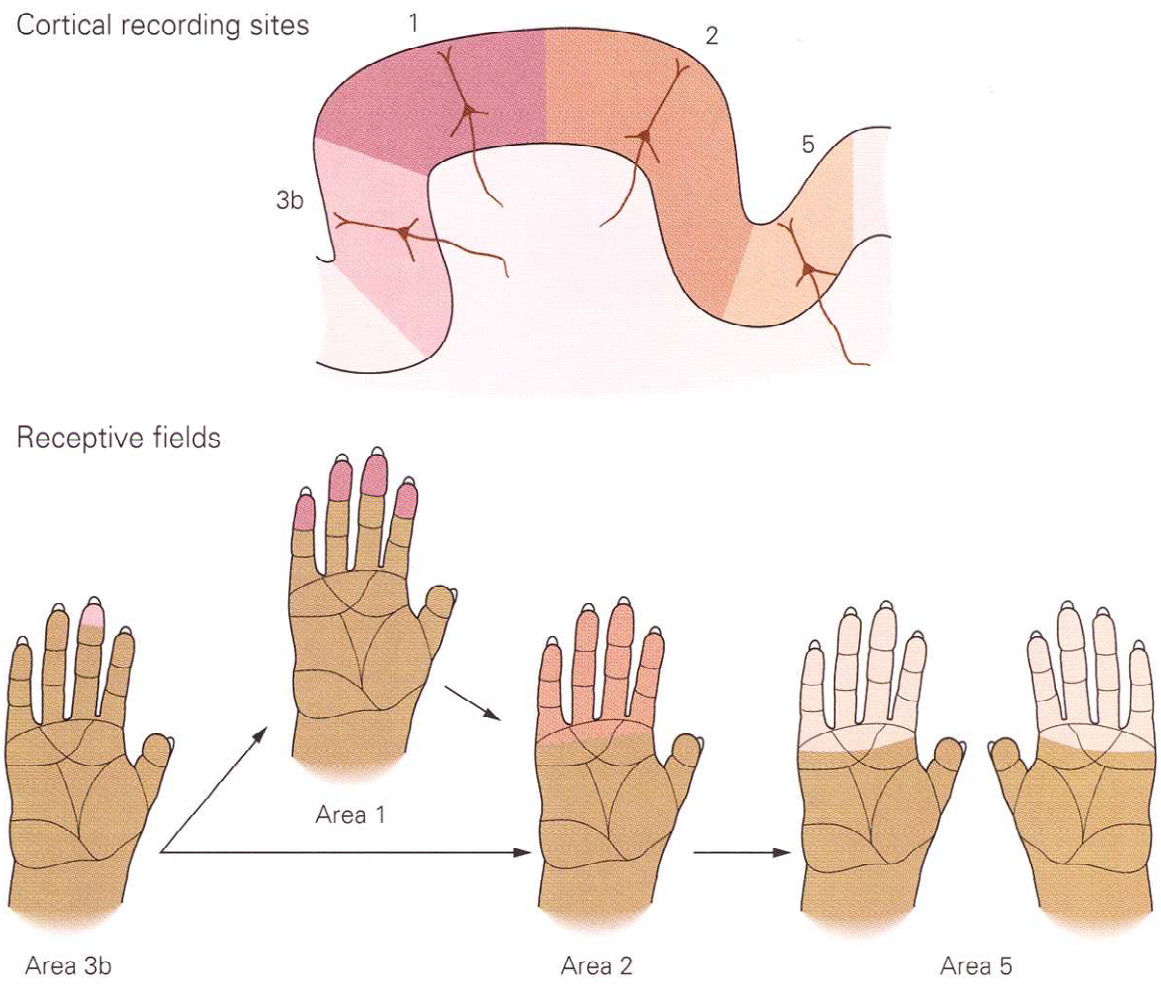

Figure 23-3 The receptive fields of neurons in the primary somatic sensory cortex are larger than those of the sensory afferents. Each of the hand figurines shows the receptive field of an individual neuron in areas 3b, 1, 2, and 5 of the primary somatic sensory cortex, based on recordings made in alert monkeys. The colored regions indicate the region of the hand where light touch elicits action potentials from the neuron. Neurons that participate in later stages of cortical processing (Brodmann's areas 1 and 2) have larger receptive fields and more specialized inputs than neurons in area 3b. The neuron illustrated from area 2 is directionally sensitive to motion toward the fingertips. Neurons in area 5 often have symmetric bilateral receptive fields at mirror image locations on the contralateral and ipsilateral hand. (Adapted from Gardner 1988, Iwamura et al. 1994.)

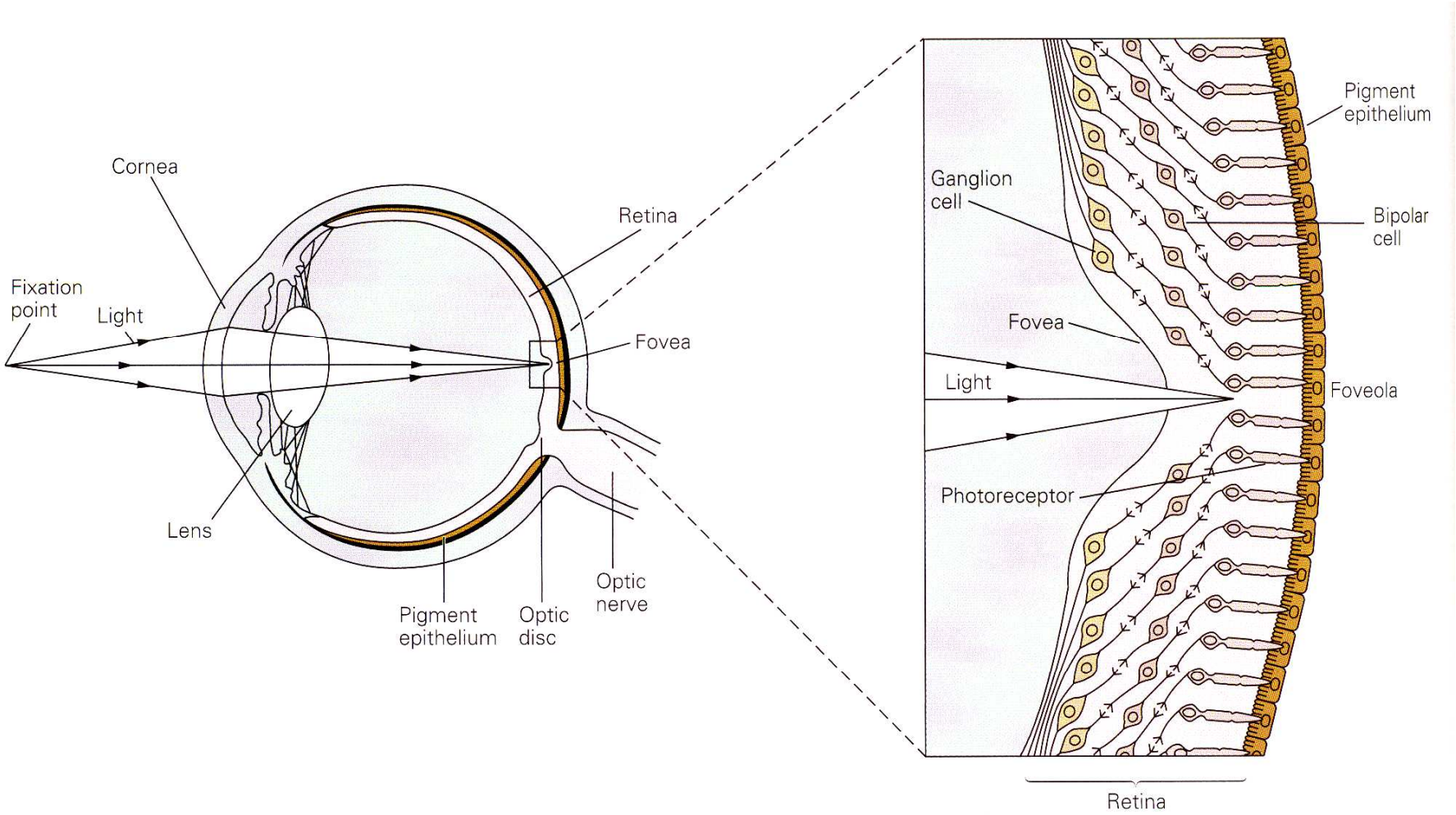

Figure 26-1 Photoreceptors are located in the retina. The location of the retina within the eye is shown at **left.** Detail of the retina at the fovea is shown on the **right** (the diagram has been simplified by eliminating lateral connections mediated by interneurons; see Figure 26-6). In most of the retina light must pass through layers of nerve cells and their processes before it reaches the photoreceptors. In the center of the fovea, or foveola, these proximal neurons are shifted to the side so that light has a direct pathway to the photoreceptors. As a result, the visual image received at the foveola is the least distorted.

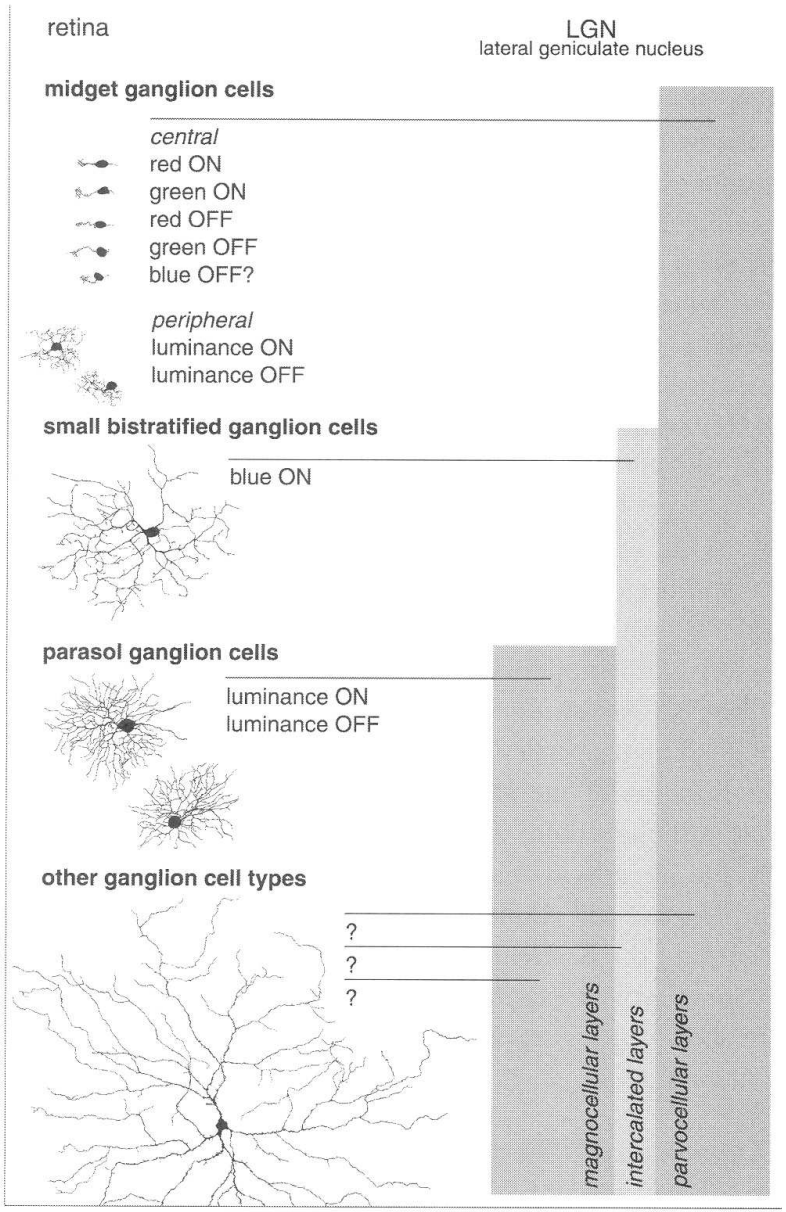

FIGURE 30.2. Examples of the morphology of some of the common ganglion cell types in the primate retina, together with their projection targets in the LGN, and some of their physiological properties (Dacey, 2000).

E. Kaplan

SELECTIVITE NEURONALE : V1

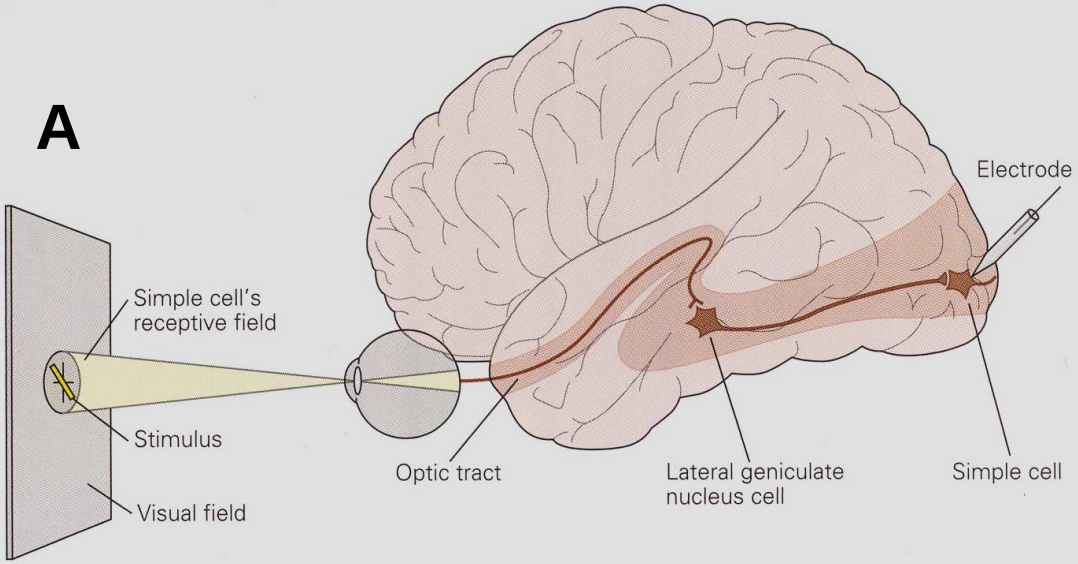

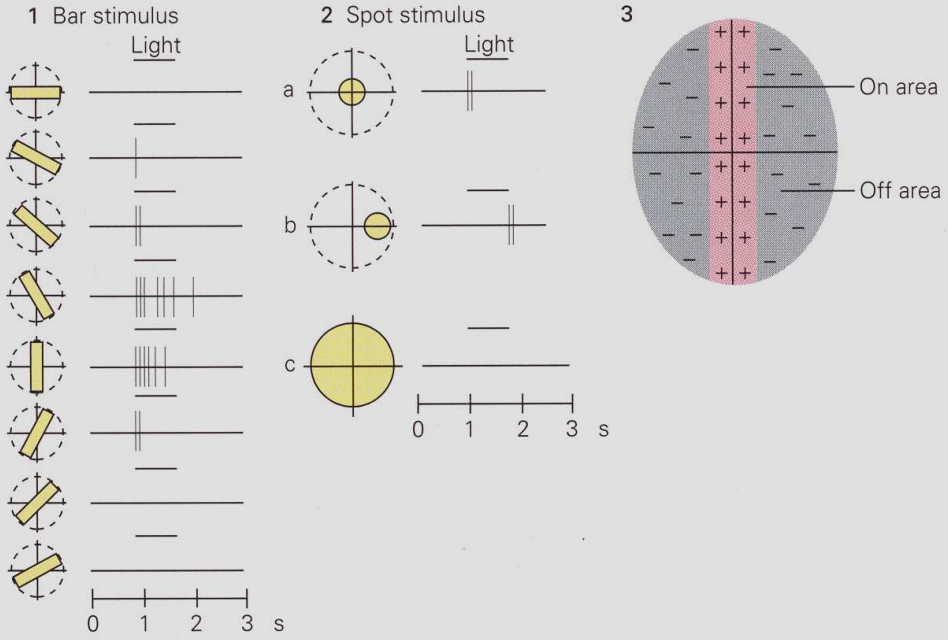

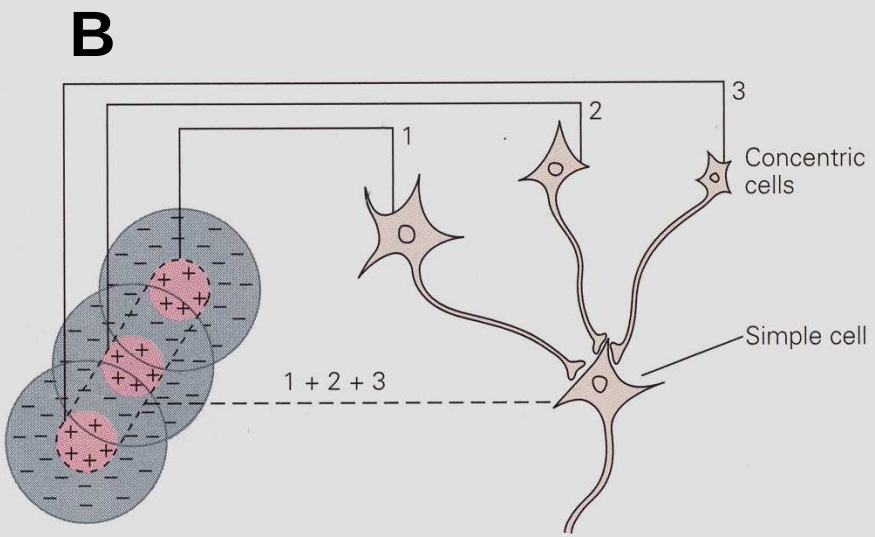

SELECTIVITE NEURONALE : V1

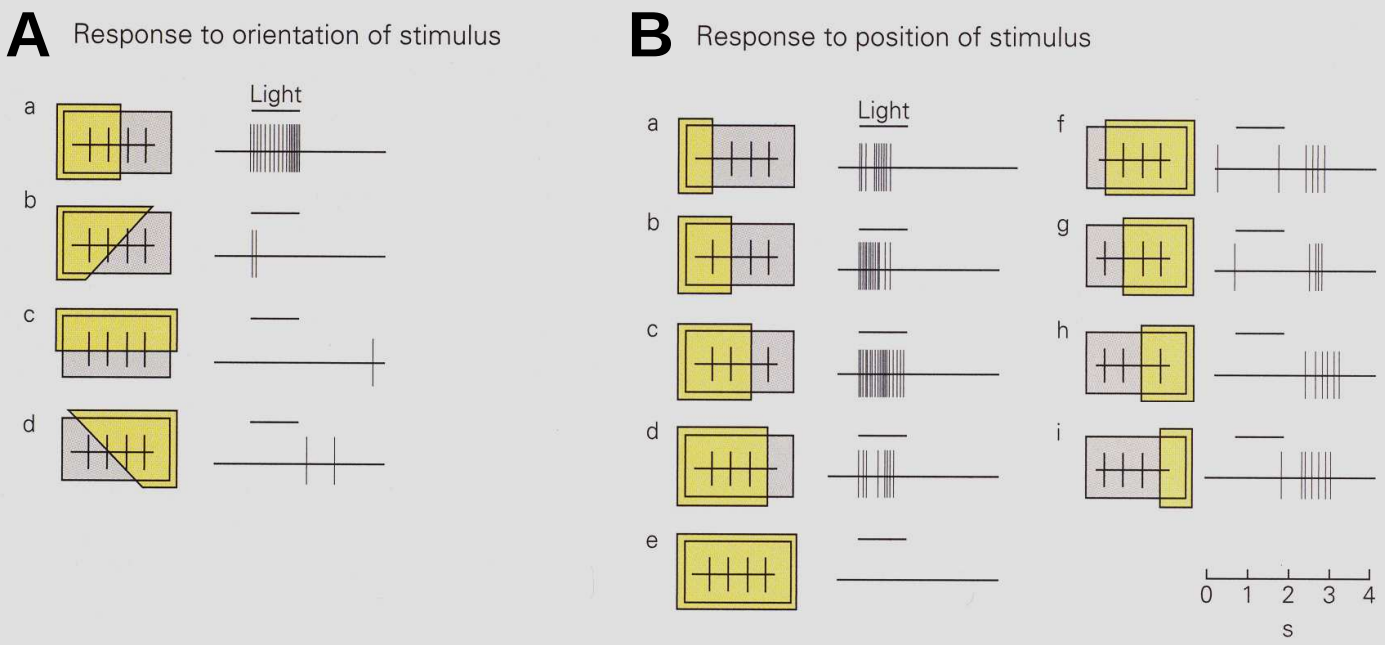

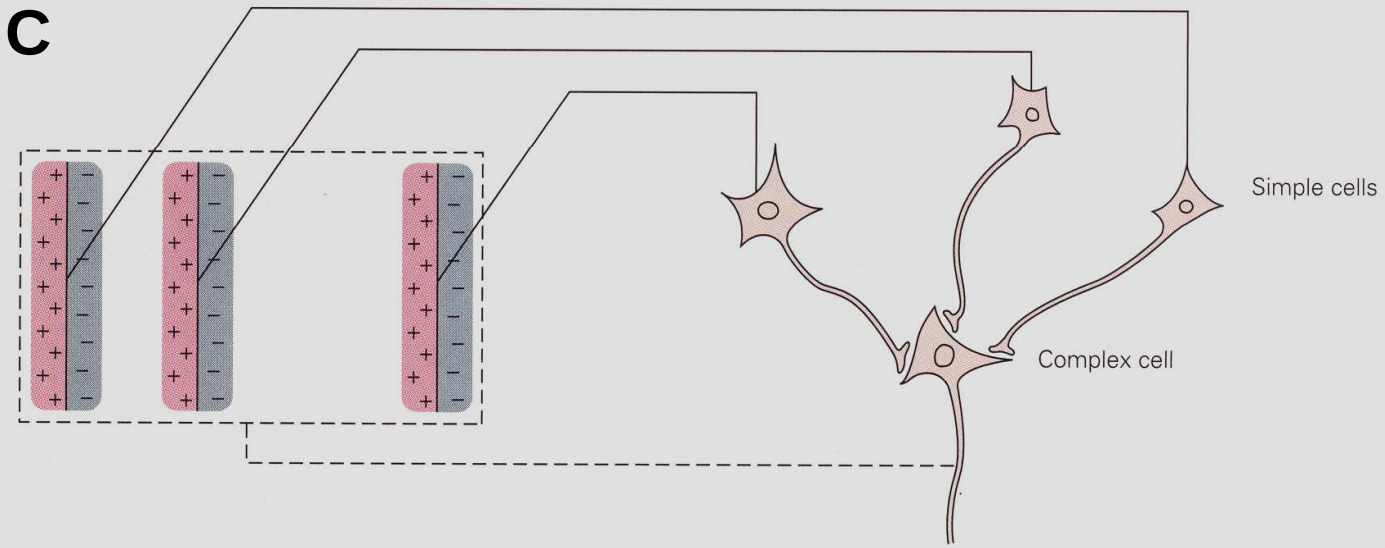

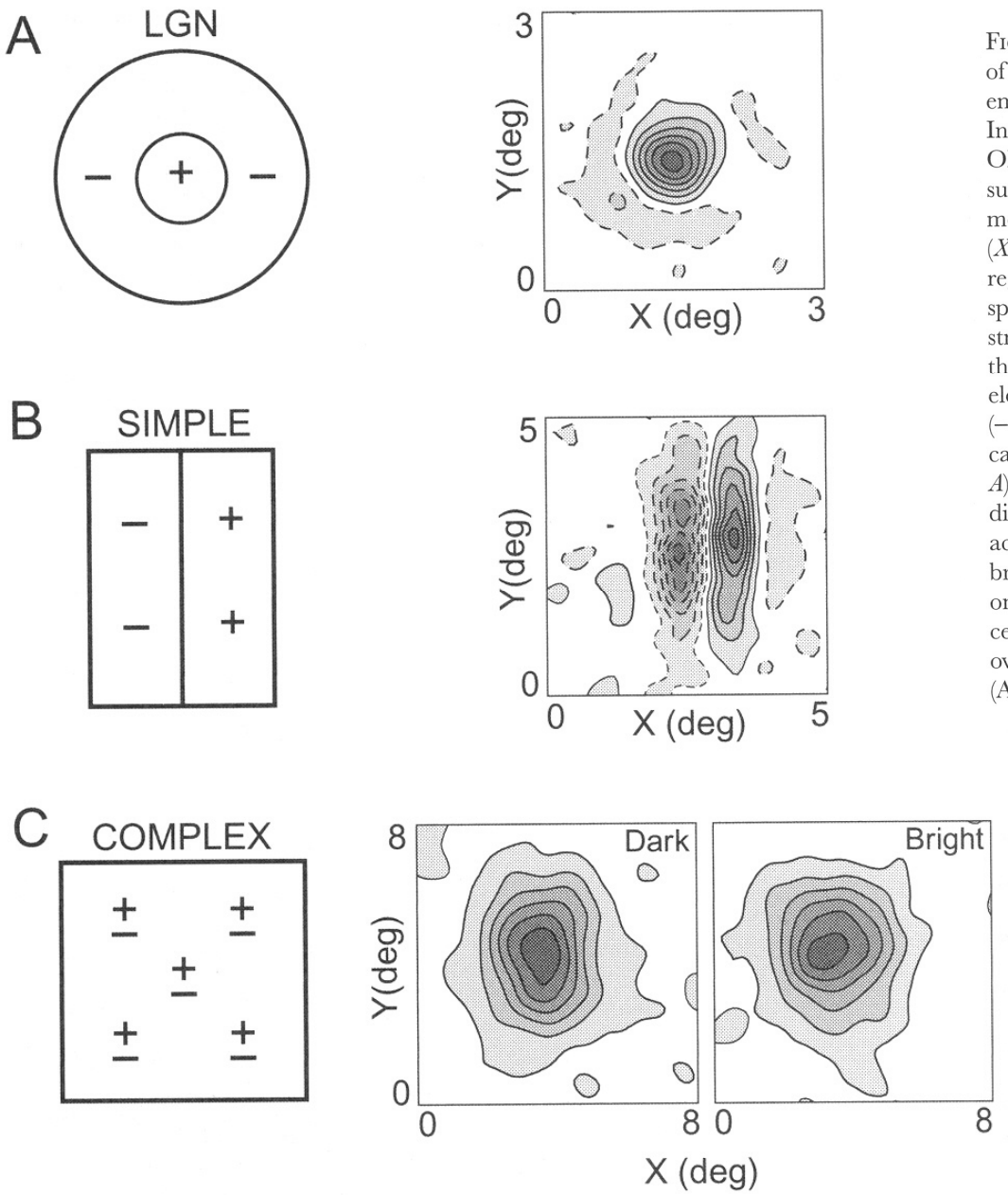

FIGURE 44.3. Spatial receptive field structure of the major classes of neurons in the geniculocortical pathway. *A*, Schematic and empirical receptive field profiles for an LGN neuron from the cat. In the traditional depiction (*left*), the receptive field has a central ON region (+) that is responsive to luminance increments and a surrounding OFF region (–) that is responsive to luminance decrements. On the right is shown a measured two-dimensional spatial (*X-Y*) receptive field profile. Solid and dashed contours represent regions of visual space in which the cell responds to bright and dark spots, respectively. Gray level saturation is proportional to response strength in each type of subregion. *B*, Depicted schematically on the left, the receptive field of a simple cell consists of alternating elongated subregions that are responsive to either bright (+) or dark (–) stimuli. A measured receptive field profile for a simple cell in cat striate cortex (area 17) is shown on the right (conventions as in *A*). *C*, Spatial receptive field structure of a complex cell. In the traditional illustration shown on the left, pluses and minuses scattered across the receptive field indicate that the cell responds to both bright and dark stimuli anywhere within the receptive field. Panels on the right show the receptive field profiles of an area 17 complex cell in cat. Because regions responsive to bright and dark stimuli overlap extensively, a separate profile is shown for each stimulus. (Adapted from DeAngelis et al., 1995a.)

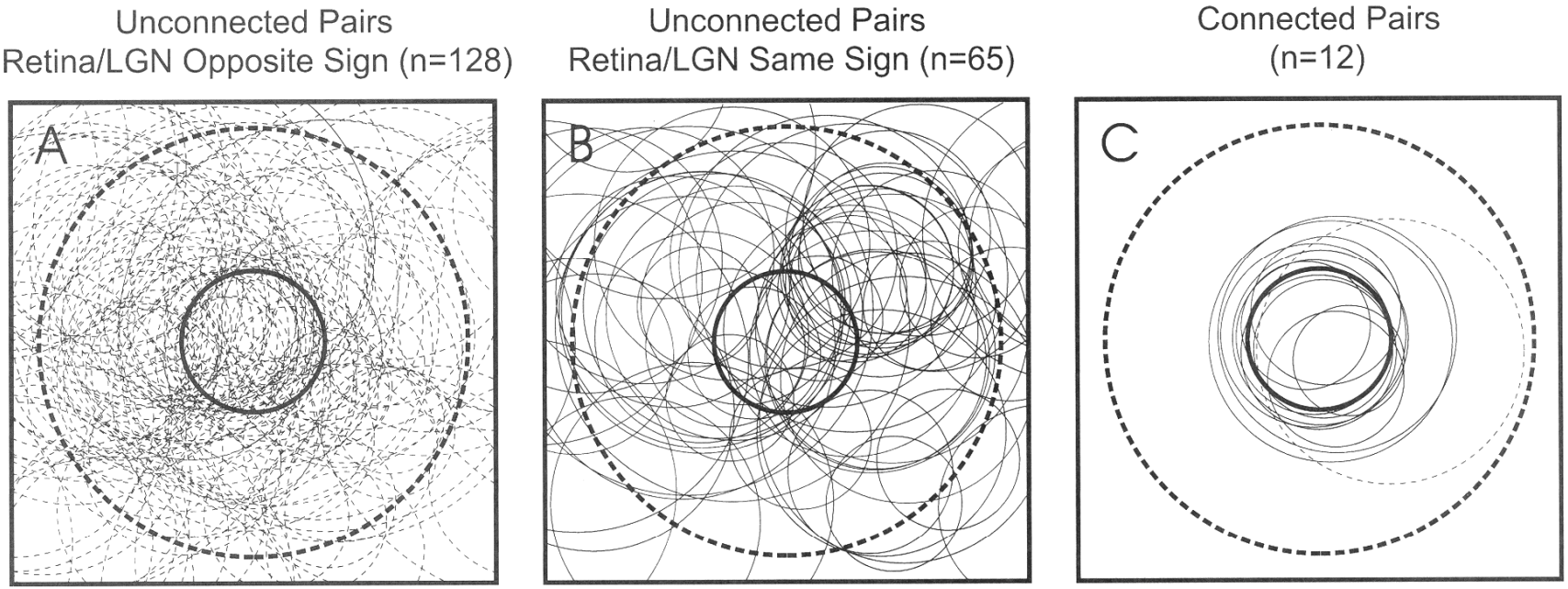

FIGURE 41.2. Summary of the specificity and strength of retinal ganglion cell input LGN neurons. Summary diagrams showing the spatial relationship of receptive fields of (*A*) unconnected retinal ganglion cells and LGN neurons with opposite (ON versus OFF) response signs, (*B*) unconnected retinal ganglion cells and LGN neurons with the same response sign, and (*C*) connected pairs. In panels *A–C*, thick circles correspond to the LGN receptive field. Receptive fields were mapped using a white-noise stimulus; connectivity was assessed using cross-correlation analysis. (From Usrey et al., 1999.)

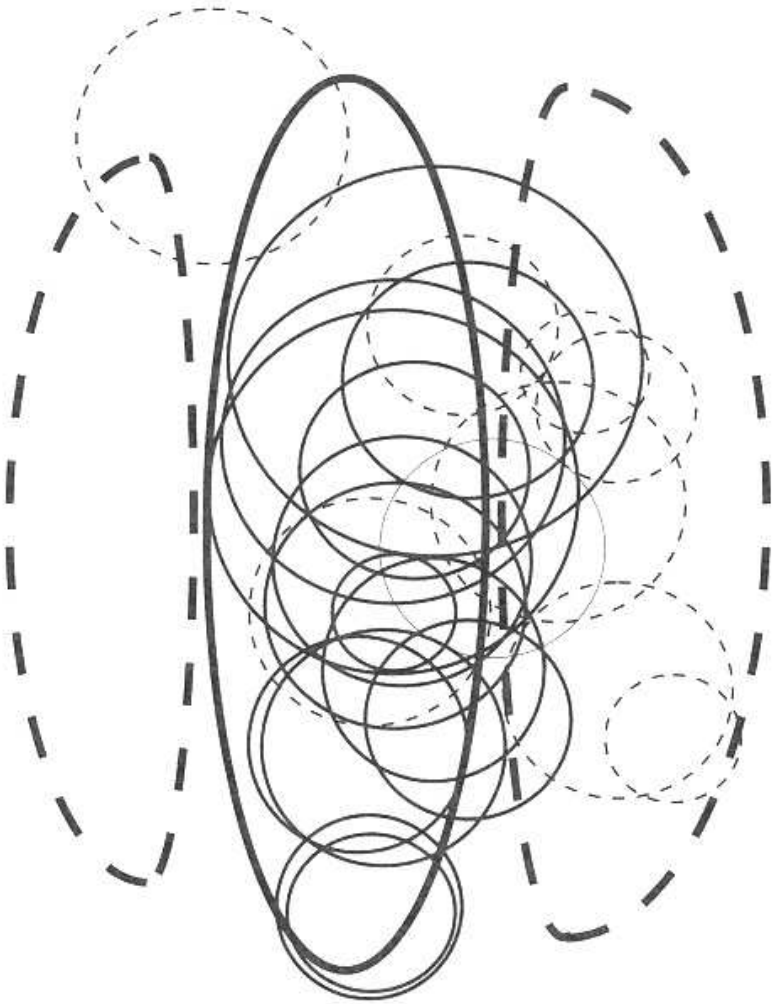

FIGURE 41.3. Summary diagram showing the relationship between the receptive fields of monosynaptically connected pairs of LGN cells and simple cells. To generate this diagram, the receptive field of each simple cell was transformed into a stylized receptive field (shown in the figure with a central subregion, indicated with solid lines, flanked by two adjacent subregions of opposite sign, indicated with dashed lines). The circles indicate the relative size, sign, and locations of the receptive field centers of monosynaptically connected LGN cells. Of the 23 pairs of connected cells (out of a total of 74 pairs recorded), very few mismatches in the sign of overlapping receptive fields were found. Receptive fields were mapped using a white-noise stimulus; connectivity was assessed using cross-correlation analysis. (From Reid and Alonso, 1995, 1996).

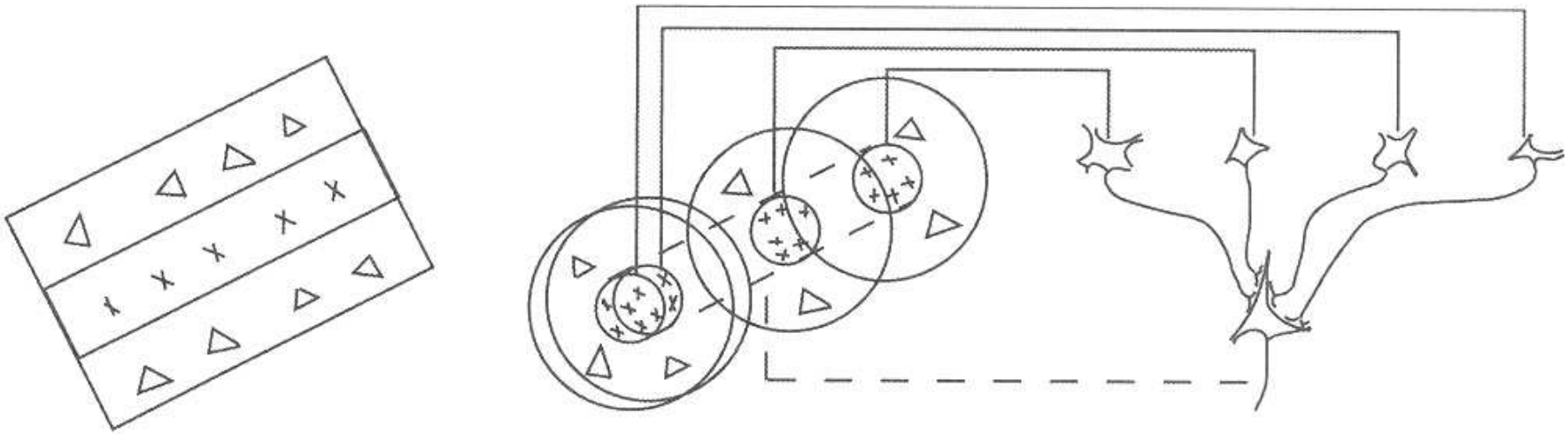

FIGURE 43.1. To the right is the receptive field of a simple cell. Crosses represent ON subfields; triangles represent OFF regions. To the left is Hubel and Weisel's proposal for how the ON subfield arises from excitatory input from ON-center geniculate relay cells whose receptive fields are aligned in a row. (Adapted from Hubel and Wiesel, 1962.)

D. Ferster

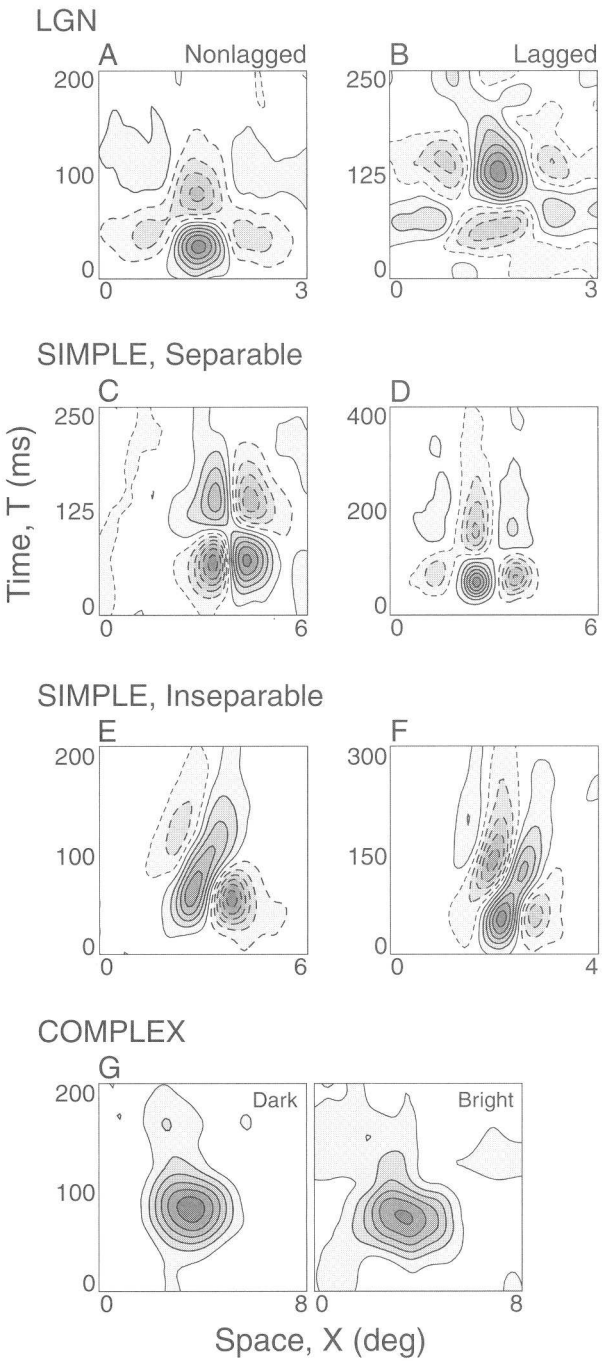

FIGURE 44.4. Linear spatiotemporal receptive field maps (X-T plots) for neurons recorded from LGN and V1 of the cat. For panels *A–F*, solid contours delimit bright-excitatory (ON) regions, whereas dashed contours indicate dark-excitatory (OFF) regions. *A*, An X-T profile is shown for a typical ON-center, *non-lagged* X cell from the LGN. For $T < 50$ msec, the receptive field profile has a bright-excitatory center and a dark-excitatory surround. However, for $T > 50$ msec, the receptive field center becomes dark-excitatory and the surround becomes bright-excitatory. *B*, An X-T plot for an ON-center, *lagged* X cell. Note that the second temporal phase of the profile is strongest. *C*, An X-T profile of a simple cell that is space-time separable. For $T < 100$ msec, the receptive field map exhibits a dark-excitatory subregion to the left of a bright-excitatory subregion. For $T > 100$ msec, each subregion reverses polarity, so that the bright-excitatory region is now on the left. *D*, Data for another simple cell with an approximately separable X-T profile. *E*, An inseparable X-T profile of a simple cell. Note how the spatial arrangement of bright- and dark-excitatory subregions (i.e., the spatial phase of the receptive field profile) changes gradually with time. *F*, Another example of an inseparable X-T profile from a simple cell for which a two-dimensional spatial profile is shown in Figure 44.3*B*. *G*, X-T profiles of the complex cell shown in Figure 44.3*C*. Responses to bright and dark stimuli are shown separately because they overlap extensively. (Adapted from DeAngelis et al., 1995a.)

SELECTIVITE NEURONALE : V1

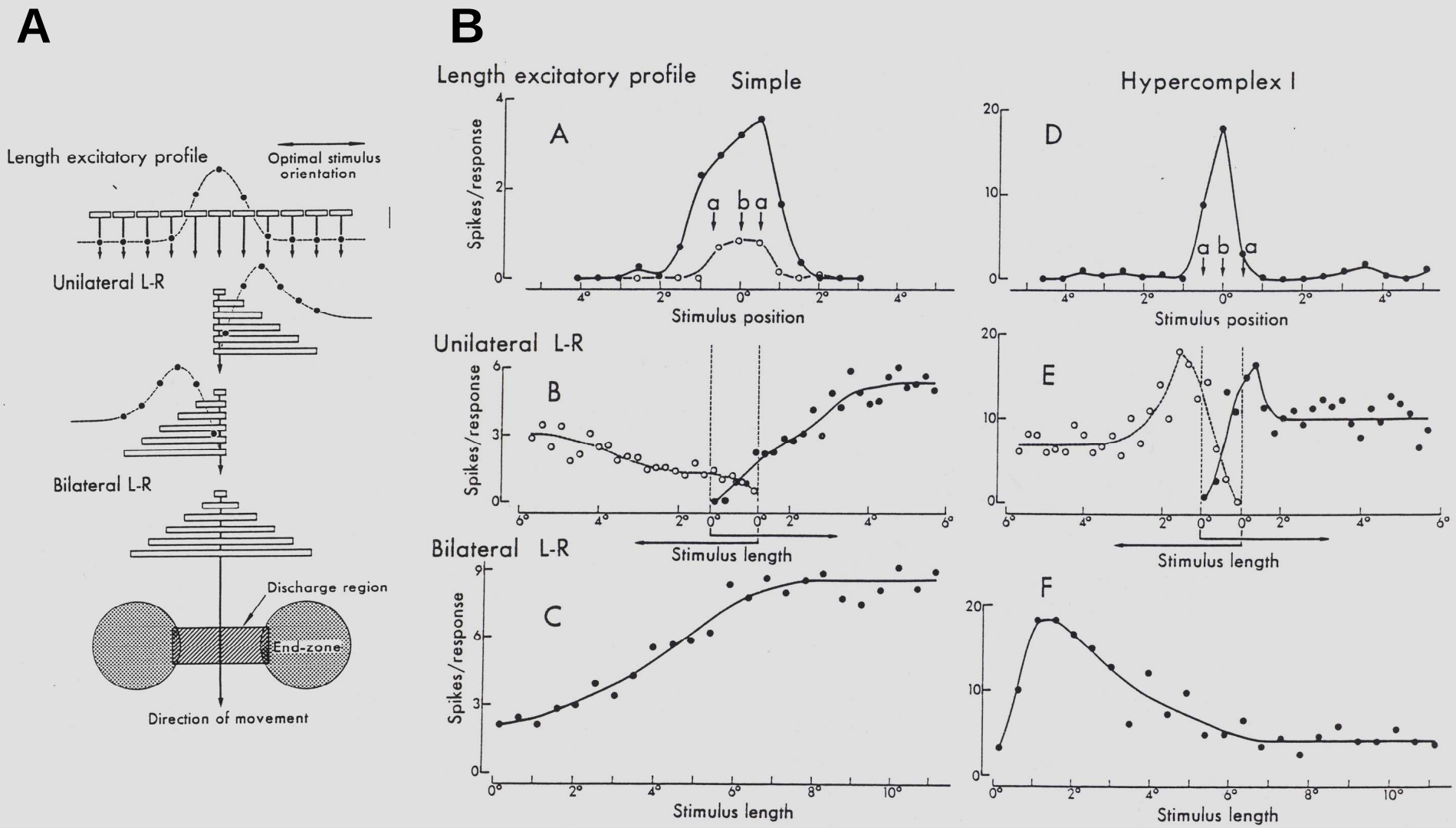

G.A. Orban et al, J. of Neurophys., ´79

Pre-Testing

Direction selectivity test

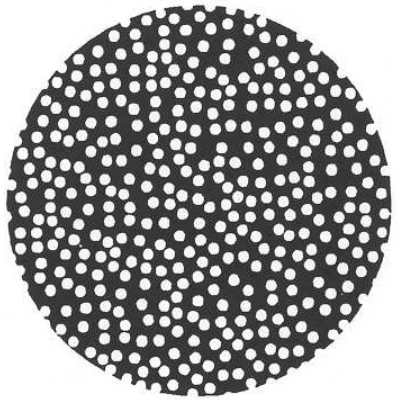

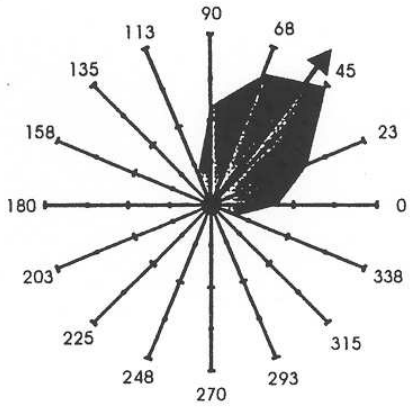

Summation Test

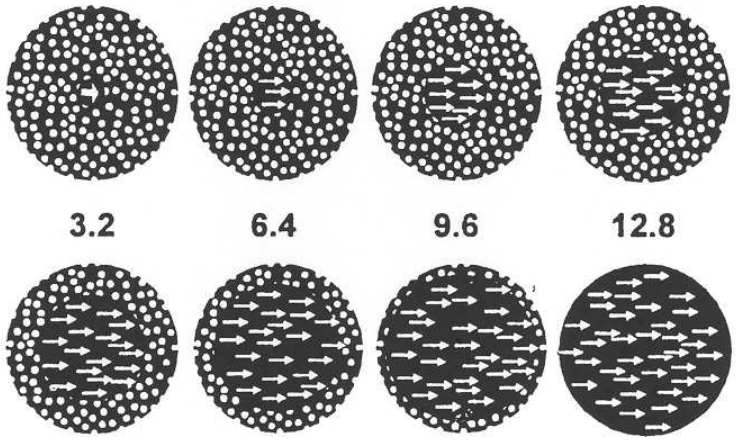

CRF Map Test

Stimulus

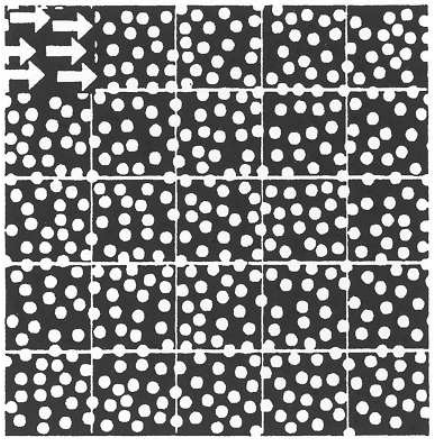

Isoresponsive contour plot

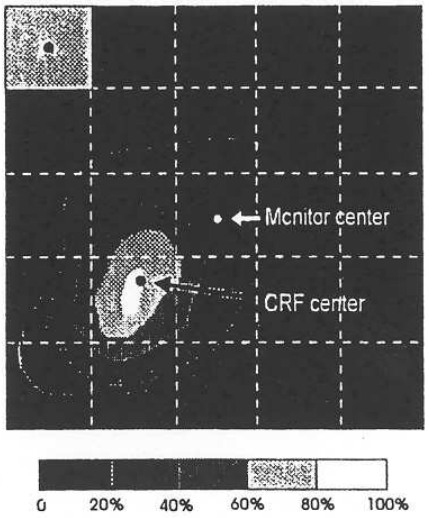

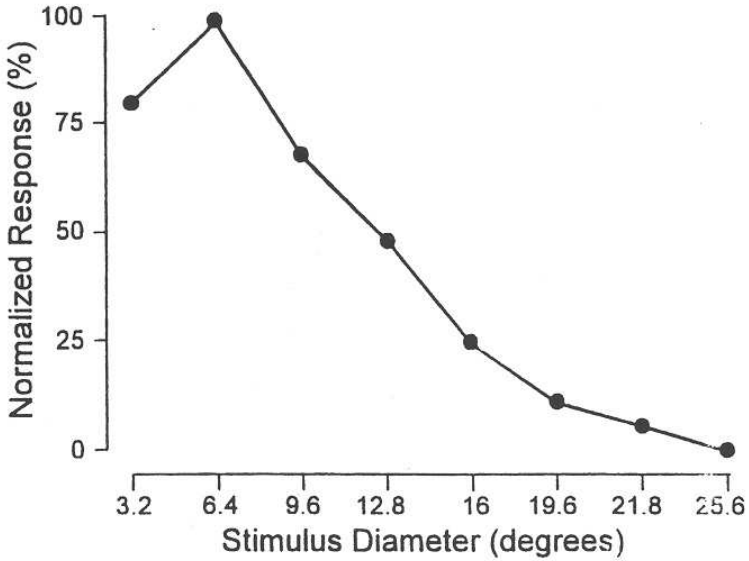

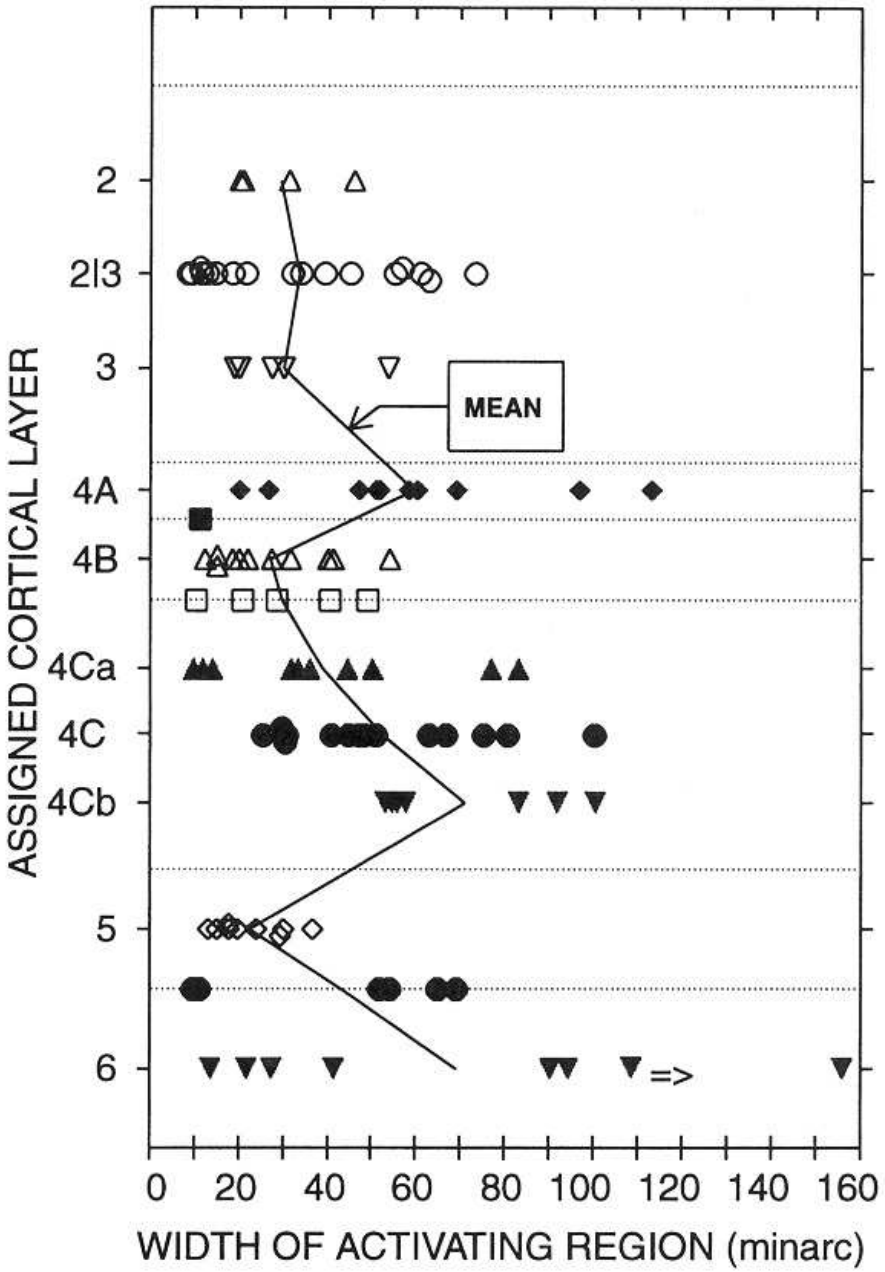

FIG. 15. Widths of ARs measured with an incremental bar. Each point represents a single cell that could be assigned to a cortical layer ($n = 107$). Solid line connects means for the different layers. Because of the limited width of the video monitor, only a minimum estimate (109 min) was obtained for 1 layer 6 cell with a large AR.

D. Max Snodderly and M. Gur, J. of Neurophys. Vol. 74, '95

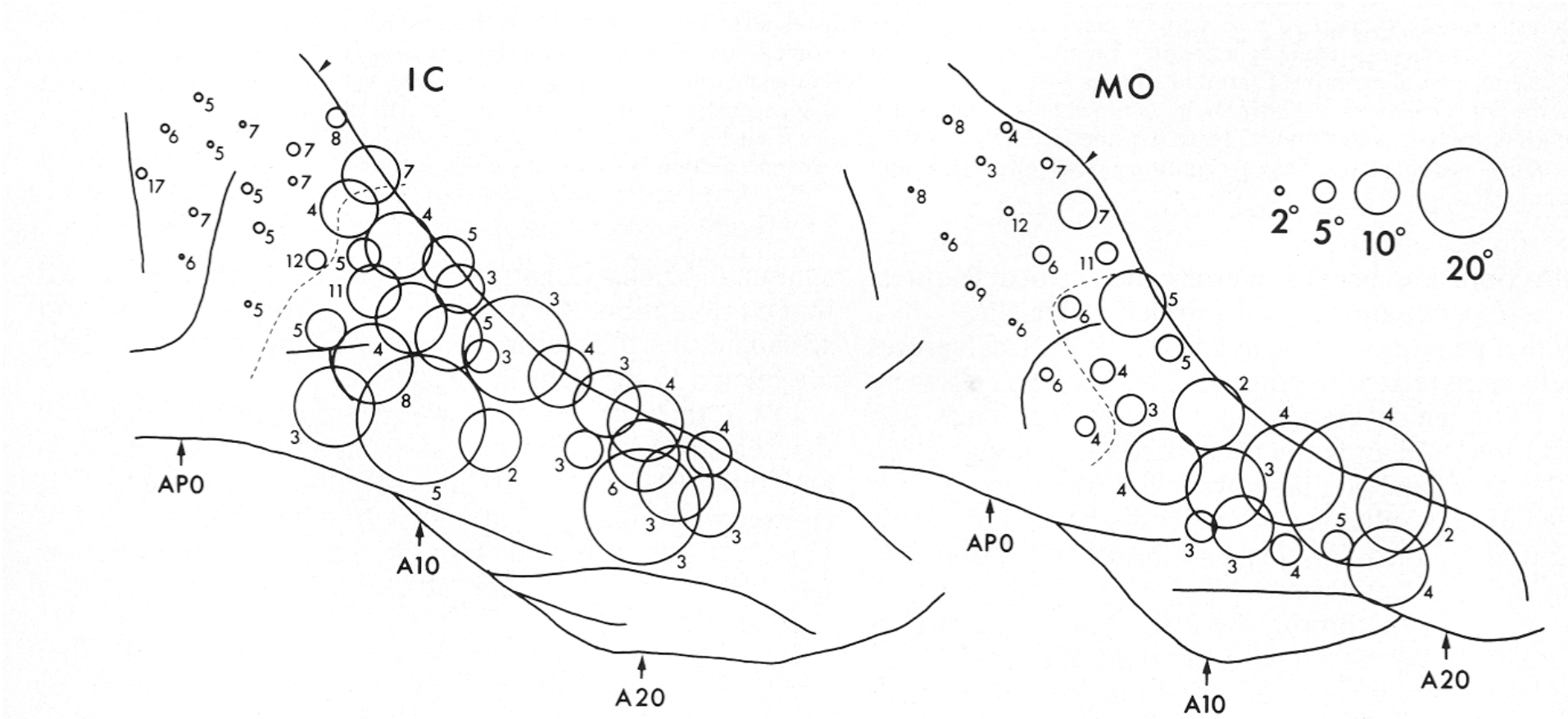

FIG. 18. Averaged square root of the area of the receptive field. Areal extent of the receptive fields was measured by assuming they were elliptic in shape, and the square root of the areal extent was averaged over cells recorded in a single penetration. Circles indicate the averaged value by their diameter and the position of the penetration by the position of their center. Figures attached to circles indicate the number of cells over which the averaging was made.

K. Tanaka et al, J. of Neurophys., Vol.66, '91

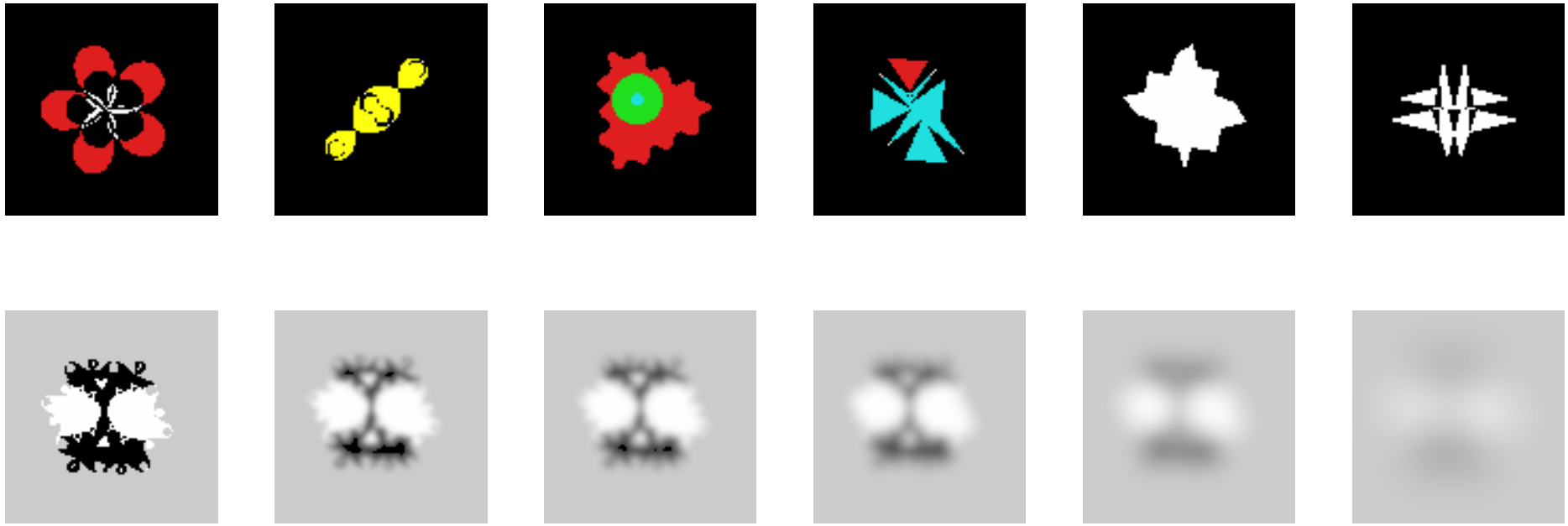

Fig. 1. Illustration of stimuli. Top: Six stimuli from the basic set of 50 stimuli used in monkeys K and J. Bottom: Stimulus from the basic set of 30 stimuli used in monkey A with its five low-pass filtered versions (left, original image; right, most filtered version).

H.op de Beeck and R. Vogels,
J. of Comp. Neurology, Vol. 426, ´00

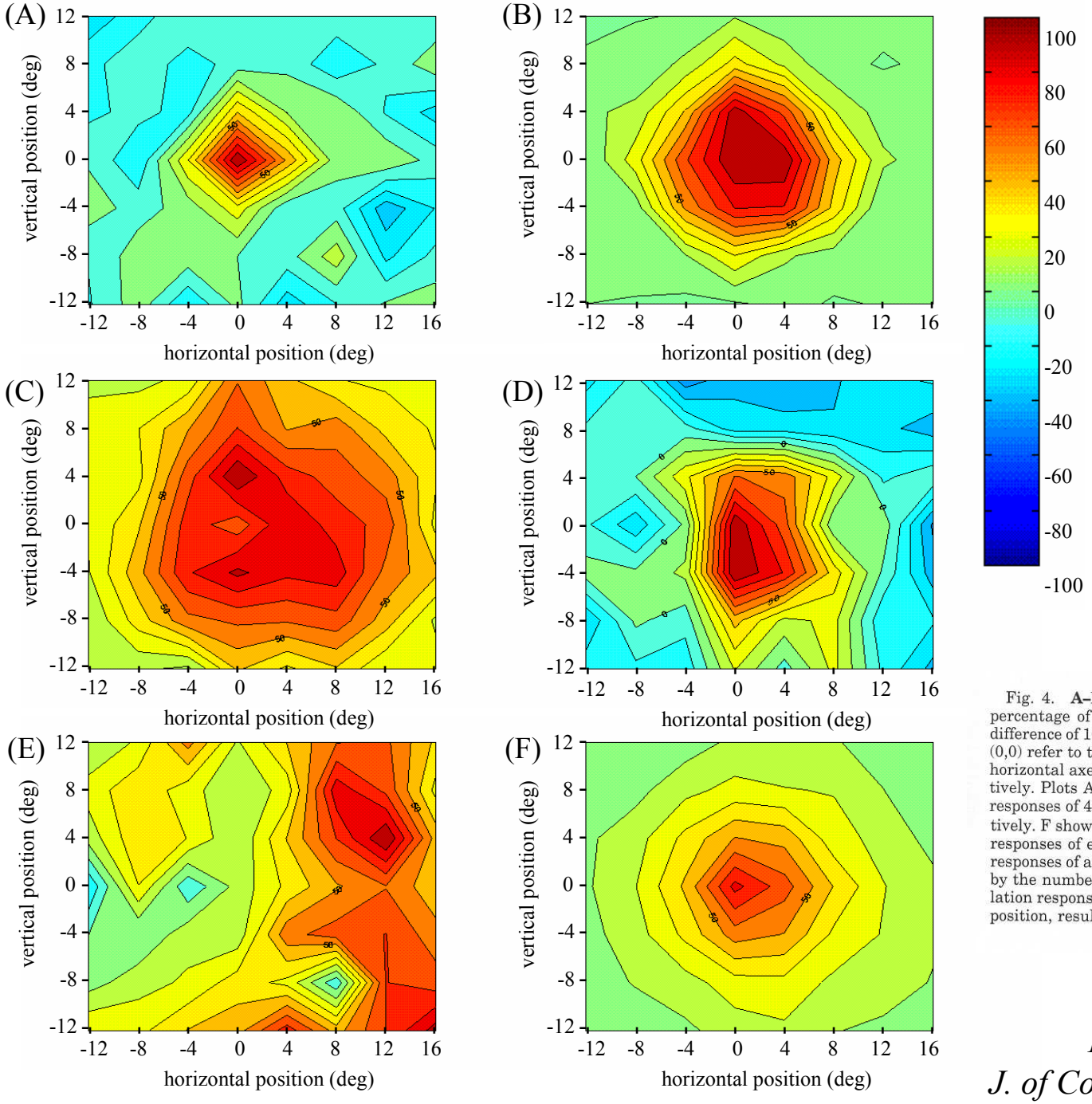

Fig. 4. **A–F:** Contour plots of receptive fields (RF) expressed in percentage of the maximum response. Each line represents a level difference of 10%, and the 50% contour line is labeled. The coordinates (0,0) refer to the foveal position. Negative indices on the vertical and horizontal axes refer to the lower and ipsilateral visual fields, respectively. Plots A–E show RFs from individual neurons with maximum responses of 48, 133, 56, 32, and 41 spikes per second in A–E, respectively. F shows the population RF obtained after normalization of the responses of each neuron to its maximum response. The normalized responses of all neurons were added at each position and then divided by the number of neurons and multiplied by 100. These mean population responses were not normalized to the response at the preferred position, resulting in a maximum at the fovea below 100.

H.op de Beeck and R. Vogels,
J. of Comp. Neurology, Vol. 426, ´00

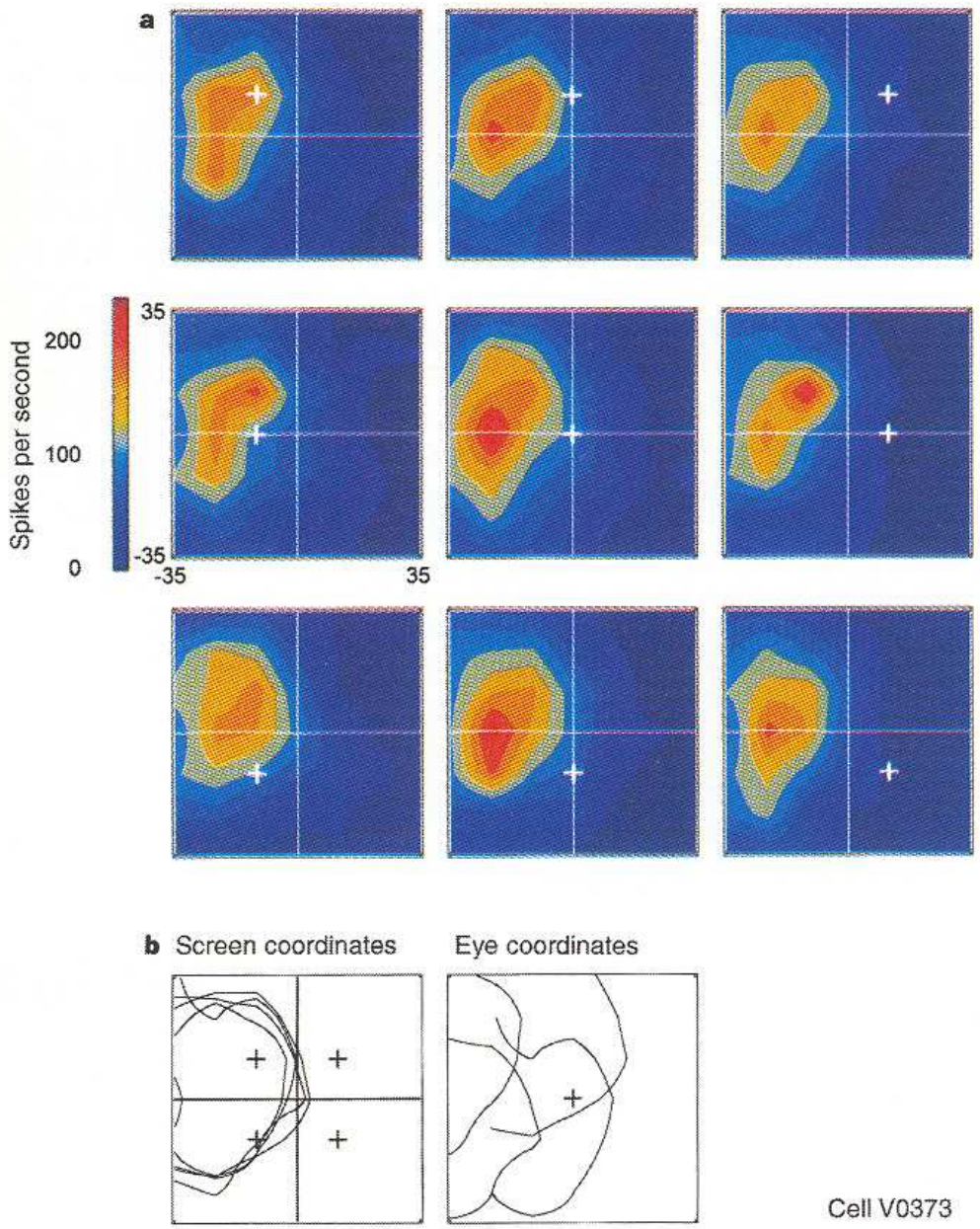

Figure 2 Single-neuron data for visual receptive field mappings in which the RF remains in the same spatial location irrespective of eye position. The RF was mapped with a white bar moving at 100 deg s^{-1} for brief intervals in the neuron's preferred direction. **a**, Colour-coded maps of the RF were constructed for each fixation position. Contour maps represent isofrequency intervals computed from linearly interpolated data matrices. Maps are displayed in screen coordinates. The small white crosses correspond to the eye position during visual stimulation; the intersection of the light horizontal and vertical lines corresponds to the straight-ahead direction in space. **b**, Contour plots for the top left, top right, bottom left and bottom right RF maps show the stimulation region from which firing rates above 50% of peak discharge were obtained. The left graph superimposes the four RF maps as they appear in screen coordinates (as in the colour-coded plots); the right graph represents the same maps but reframed in eye coordinates (relative to the fovea).

J-R. Duhamel et al, Nature, vol.389, ´97

A

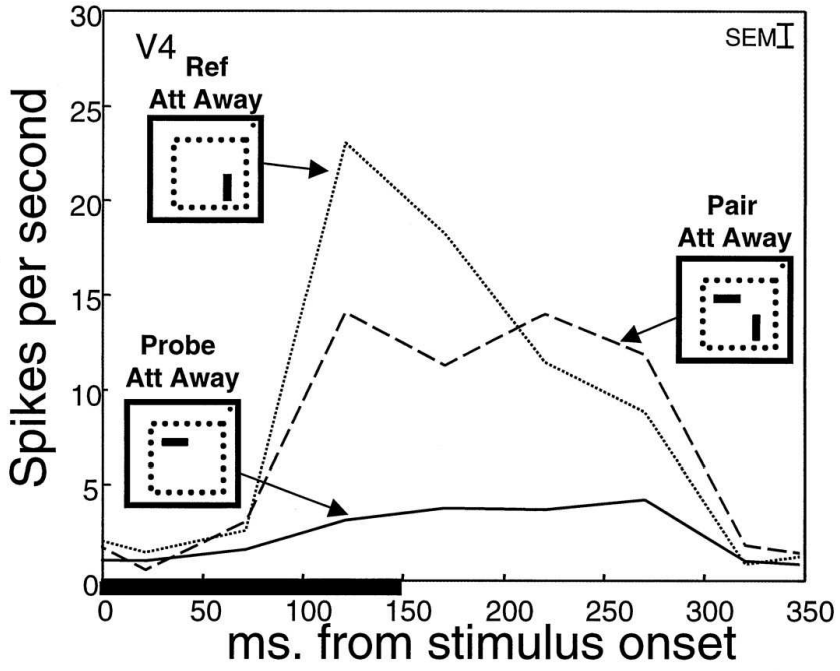

B

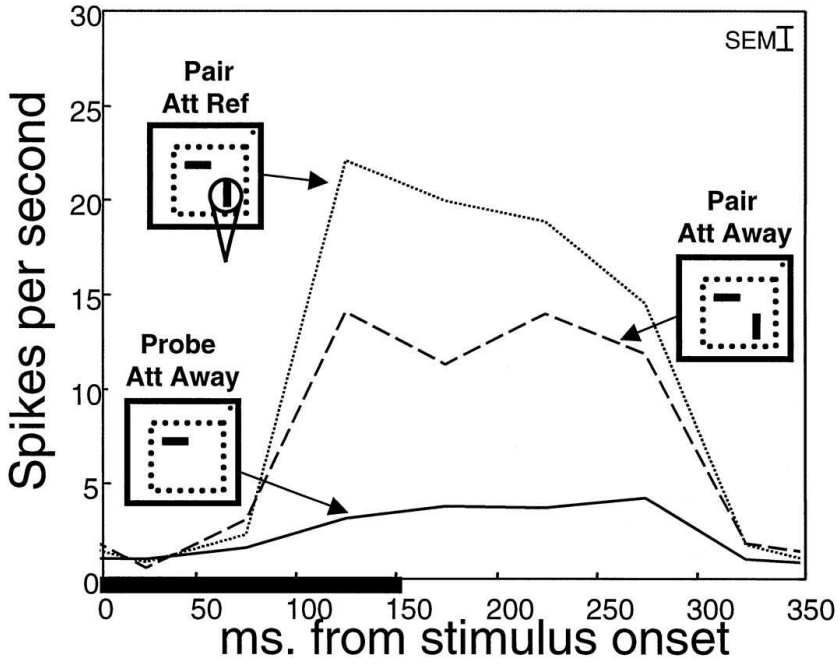

Attention filtering out the effect of a suppressive probe in V4. The format is identical to that in Figure 6. *A*, With attention directed away, the response to the reference stimulus (*dotted line*) was suppressed (response to pair, *dashed line*) by the addition of the probe (response to probe, *solid line*). *B*, Attention to the reference stimulus drove the pair response (*dotted line*) toward the response elicited by the unattended reference stimulus presented alone (*dotted line* in *A*).

J.H. Reynolds et al, J. of Neurosci., Vol.19, ´99

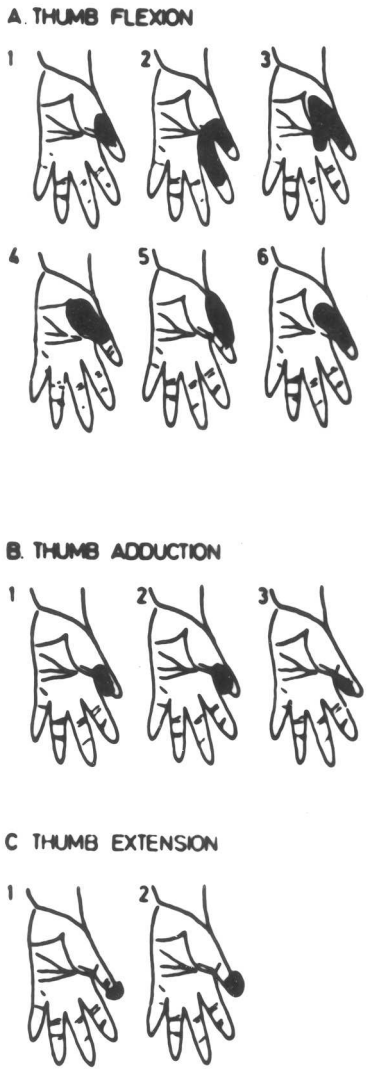

A.: 1. Thumb flexion
2. Thumb extension
3. Thumb extension, thenar pressure

B.: 1. Thumb movement, all directions
2. Extension dig. II

C.: 1. Thumb extension
2. Thumb extension
3. Thumb extension and flexion, pressure forearm muscles
4. Deep pressure, thenar
5. Deep pressure, thenar

Fig. 3. ***Summary of receptive fields and adequate stimuli*** of all driven cells encountered within efferent zones where thumb flexion (A), thumb adduction (B) or thumb extension (C) were produced by ICMS at threshold stimulus strengths (<10 μa). The receptive fields of cells activated by tactile stimuli (S-cells) are shown in figurines on the left. The type and location of the adequate stimulus for activation of cells driven by deep receptors (D-cells) are listed on the right

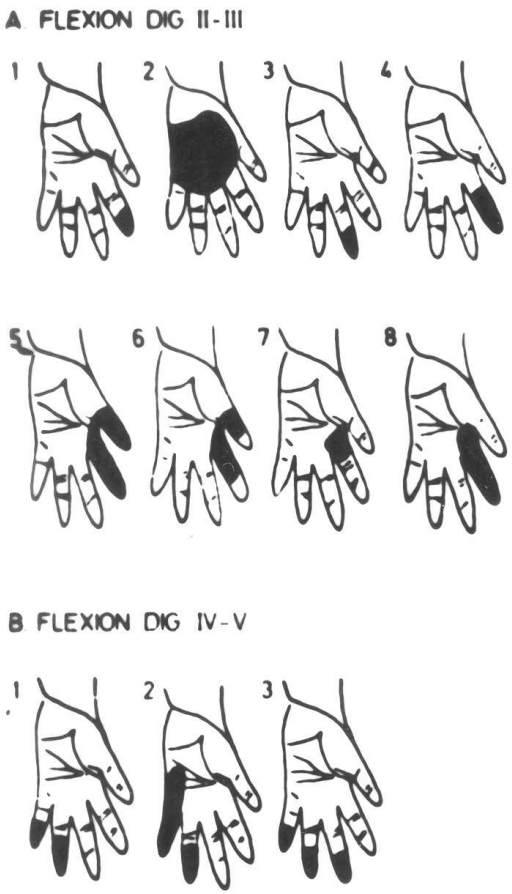

A.: 1. Flexion dig. II
2. Extension dig. III, pressure forearm muscles
3. Extension dig. II
4. Extension dig. II—III
5. Inhibited by extension dig. II—V and deep pressure of palm

B.: 1. Extension dig. IV—V
2. Extension dig. IV—V
3. Extension dig. V, pressure forearm muscles
4. Inhibited by extension dig. II—V and deep pressure of palm
5. Deep pressure, hand

C.: 1. Extension dig. III—IV
2. Extension dig. III
3. Extension dig. II—IV
4. Deep pressure, hand
5. Deep pressure, forearm
6. Deep pressure dig. III

Fig. 4. ***Summary of receptive fields and adequate stimuli*** **of all driven cells found within efferent zones producing flexion of dig. II—III (A), flexion of dig. IV—V (B), and extension of dig. II—V (C) at threshold stimulus strength <10 μa. For further details, see legend, Fig. 3. No. 8-cells were found in zones producing finger extension**

SELECTIVITE NEURONALE

Le champ récepteur et la sélectivité neuronale

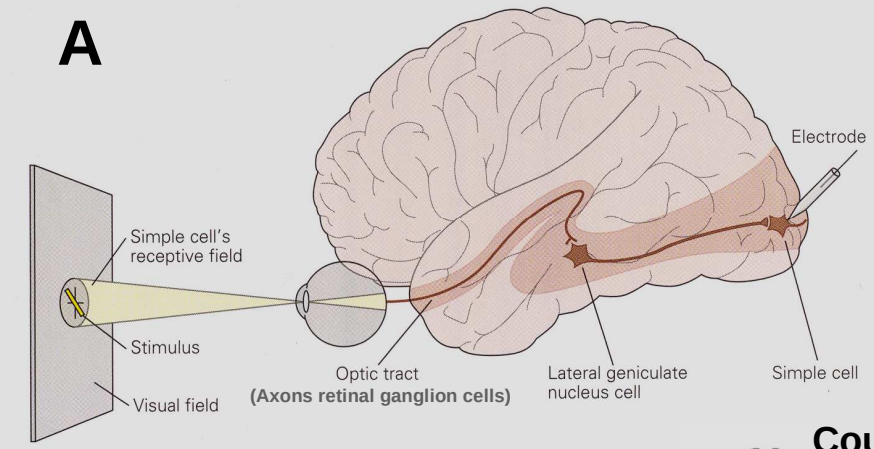

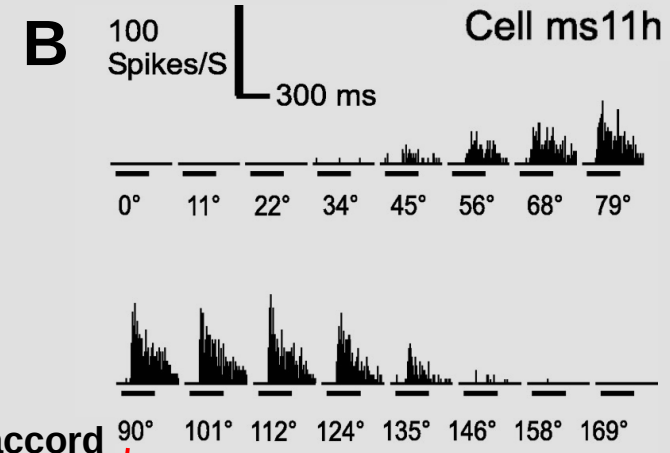

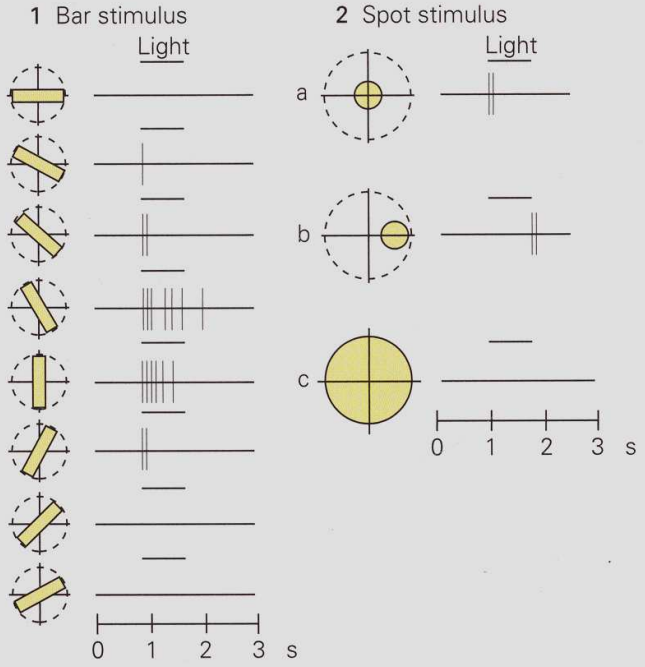

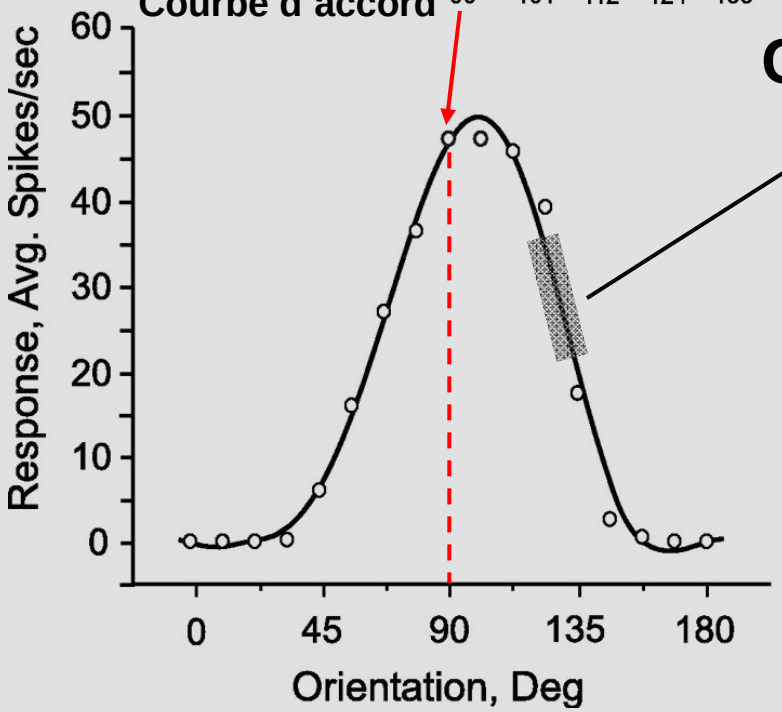

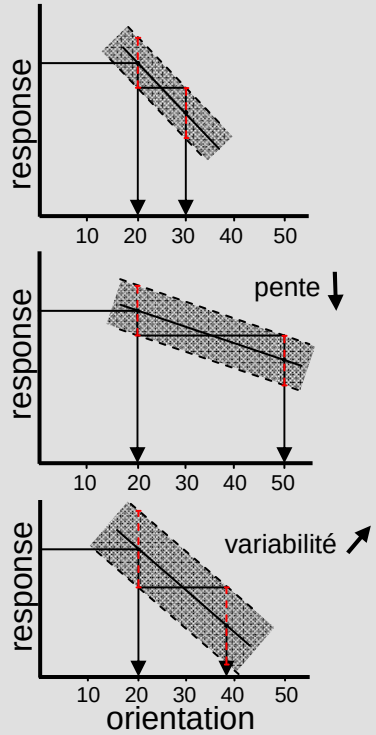

Organisation colonnaire : physiologie

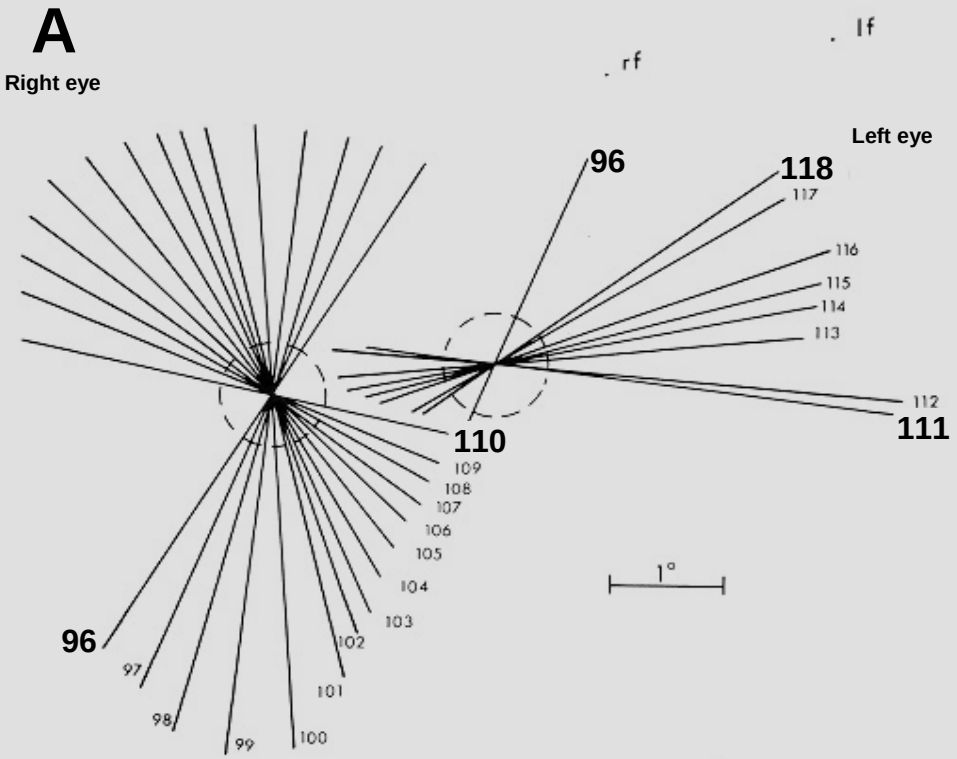

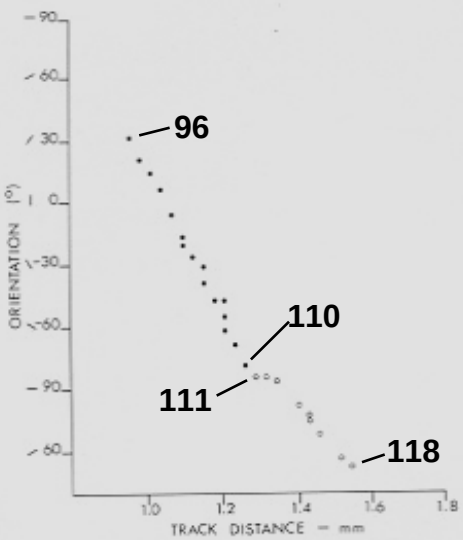

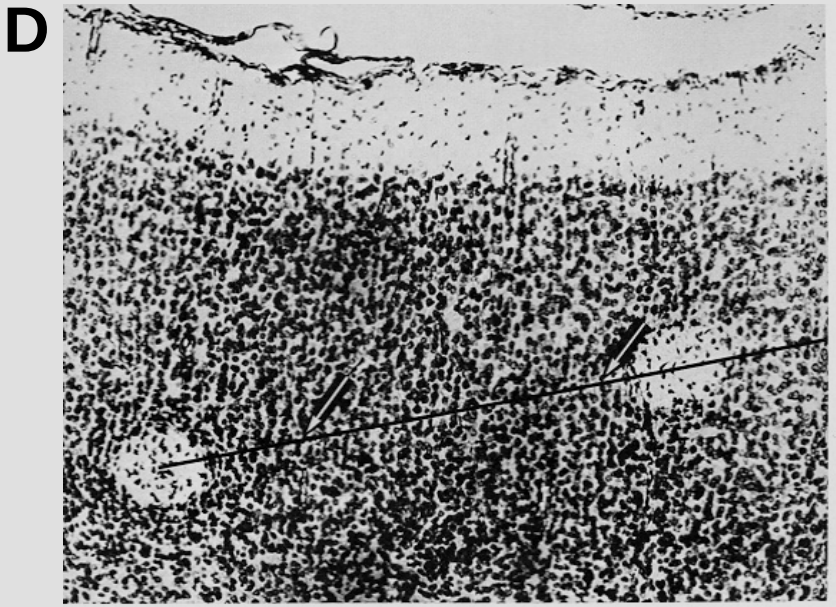

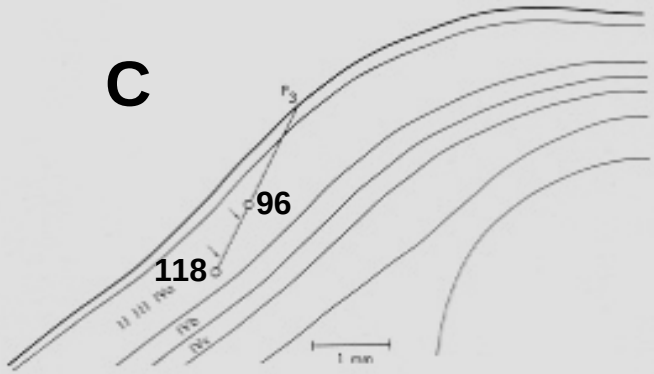

Plasticité corticale, développementale : dominance oculaire

A

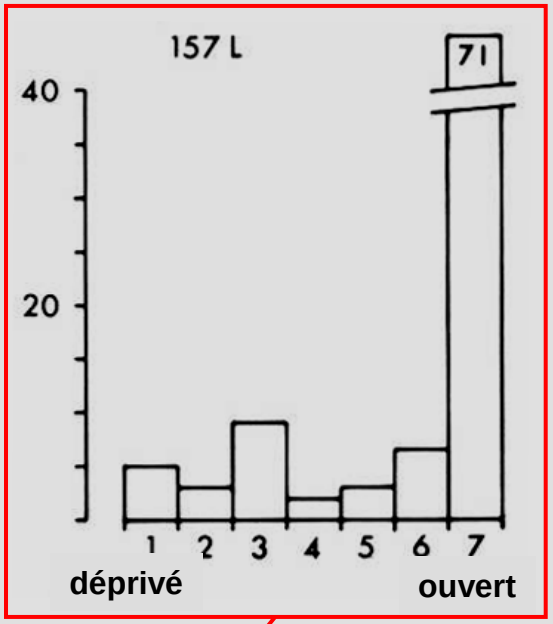

B

C

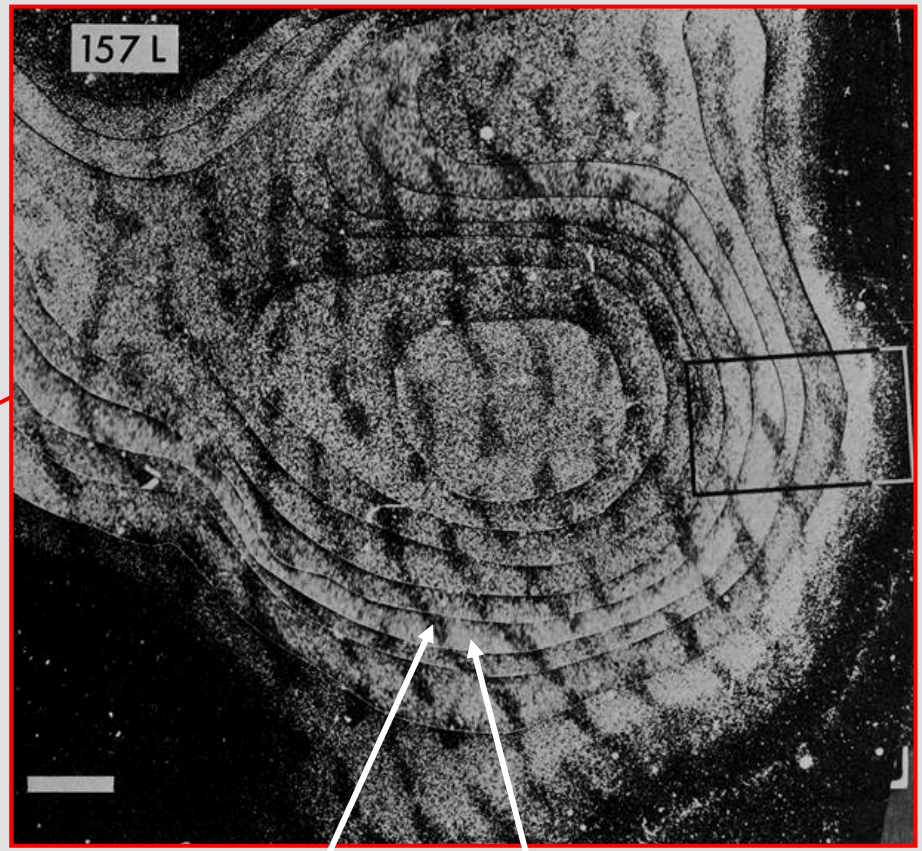

Plasticité corticale adulte : apprentissage visuel

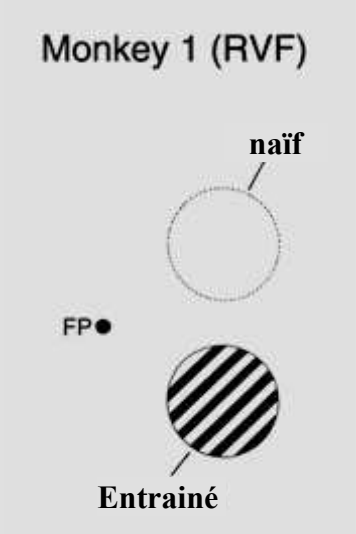

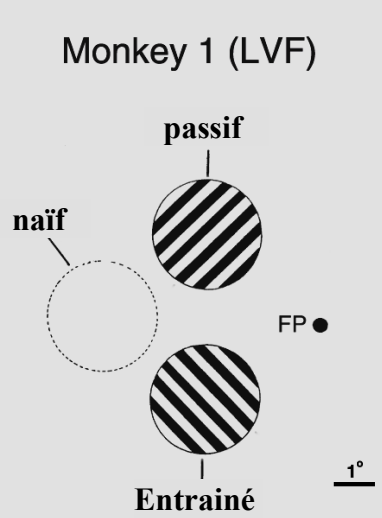

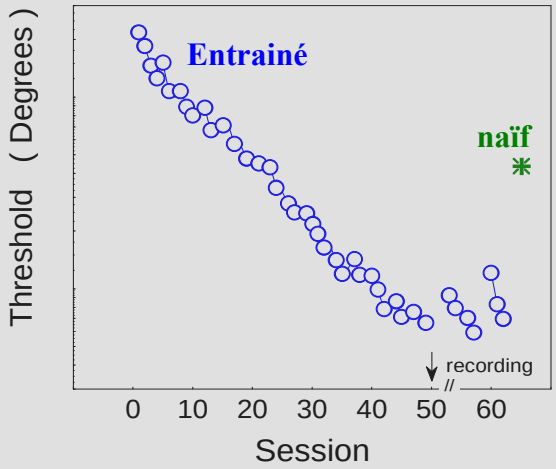

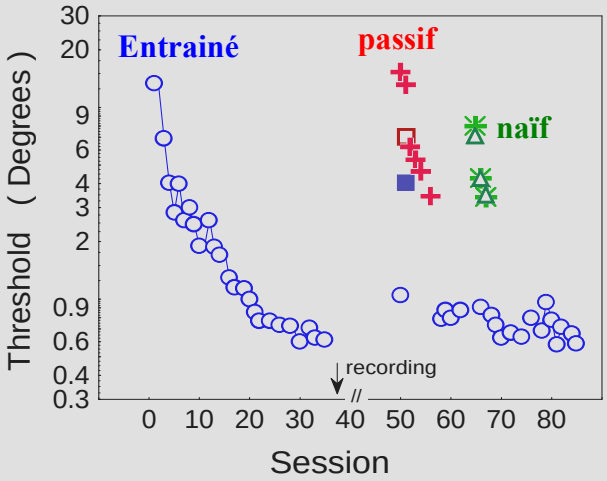

Plasticité corticale adulte : modification des neurones les plus informatifs

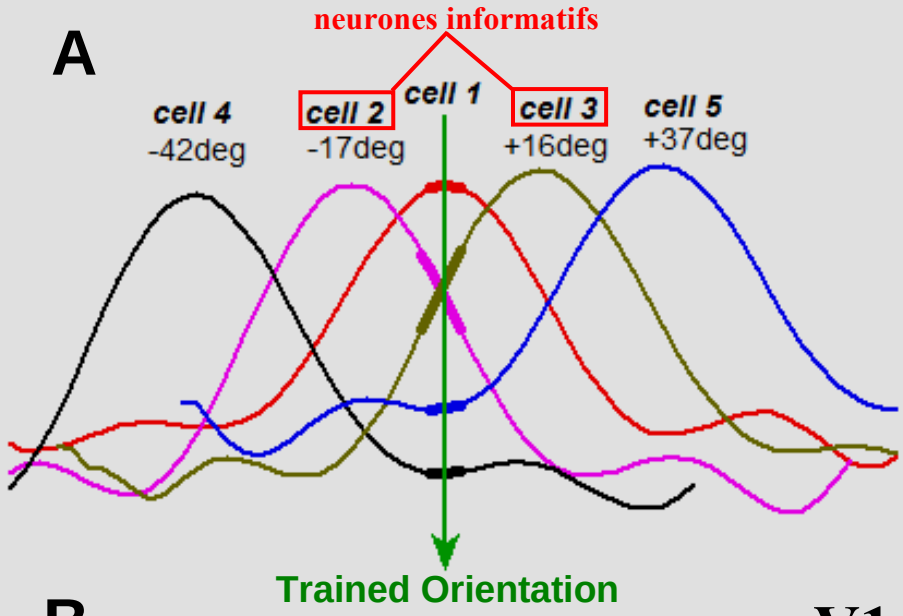

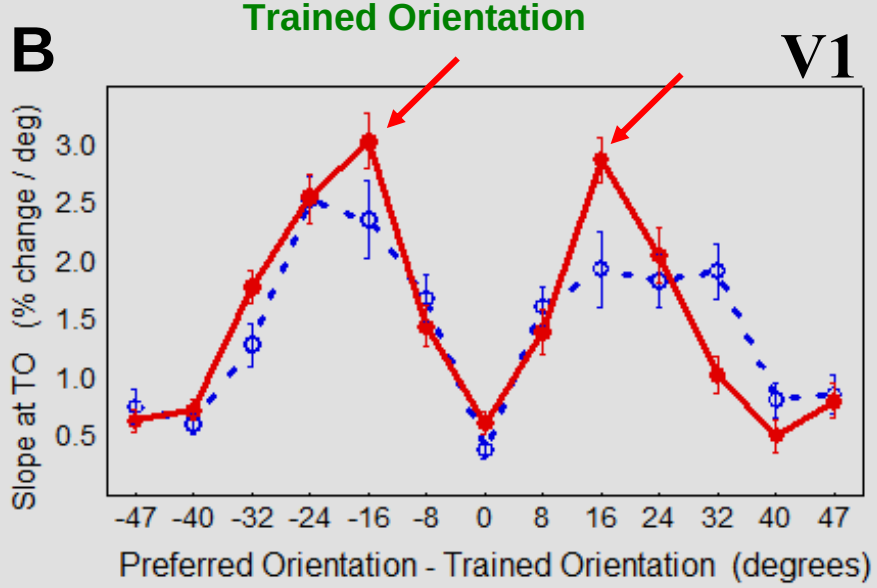

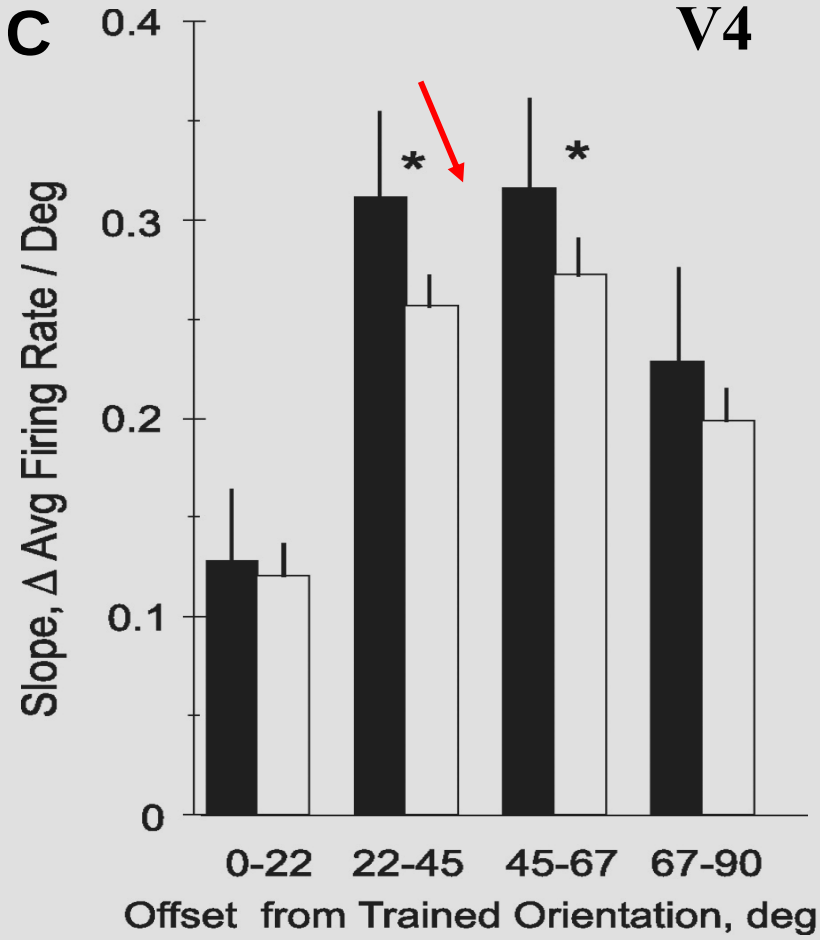

SELECTIVITE NEURONALE : MT/V5

A

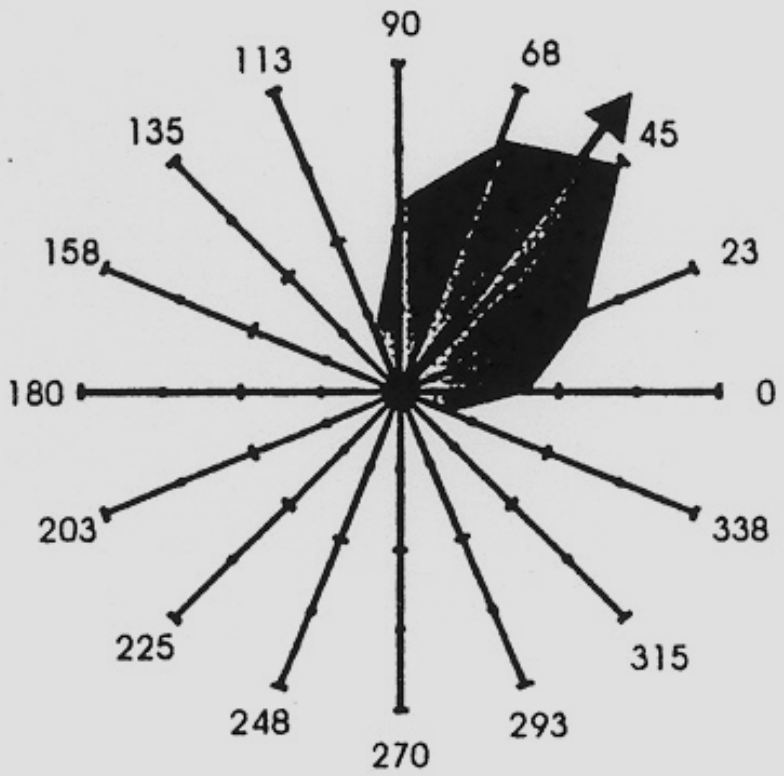

B

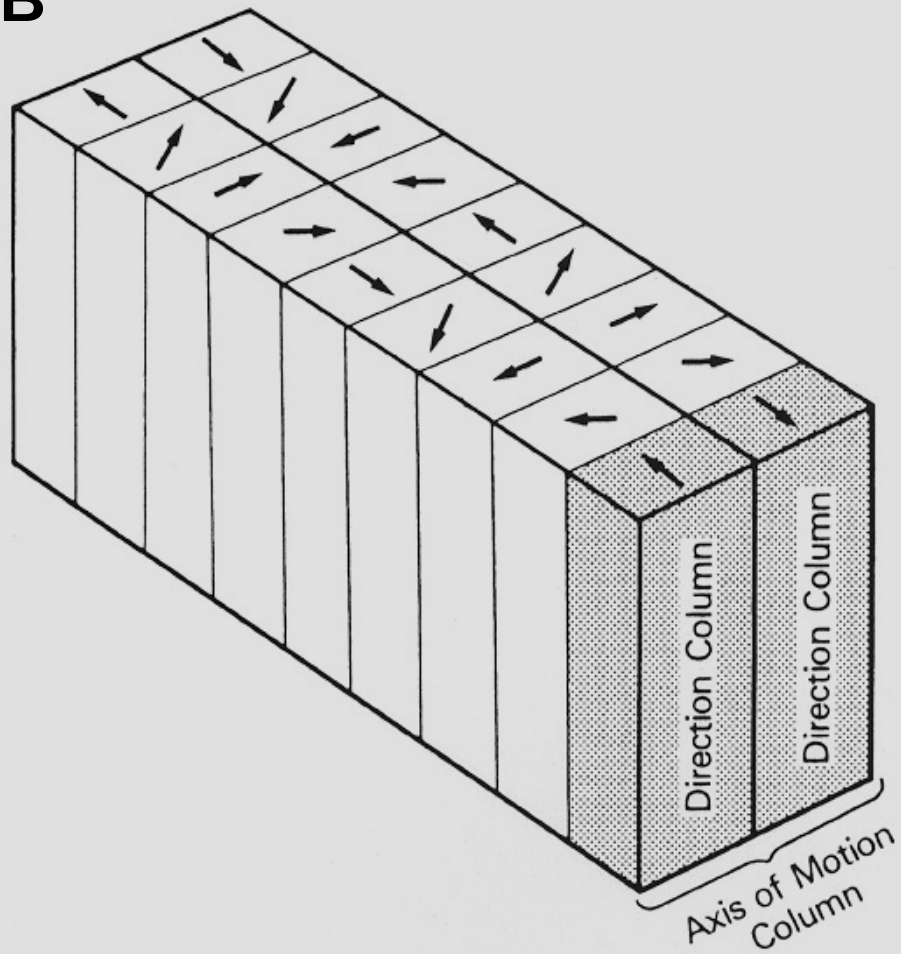

V.B. Mountcastle, Brain, vol. 120, ´97

SELECTIVITE NEURONALE : MSTd

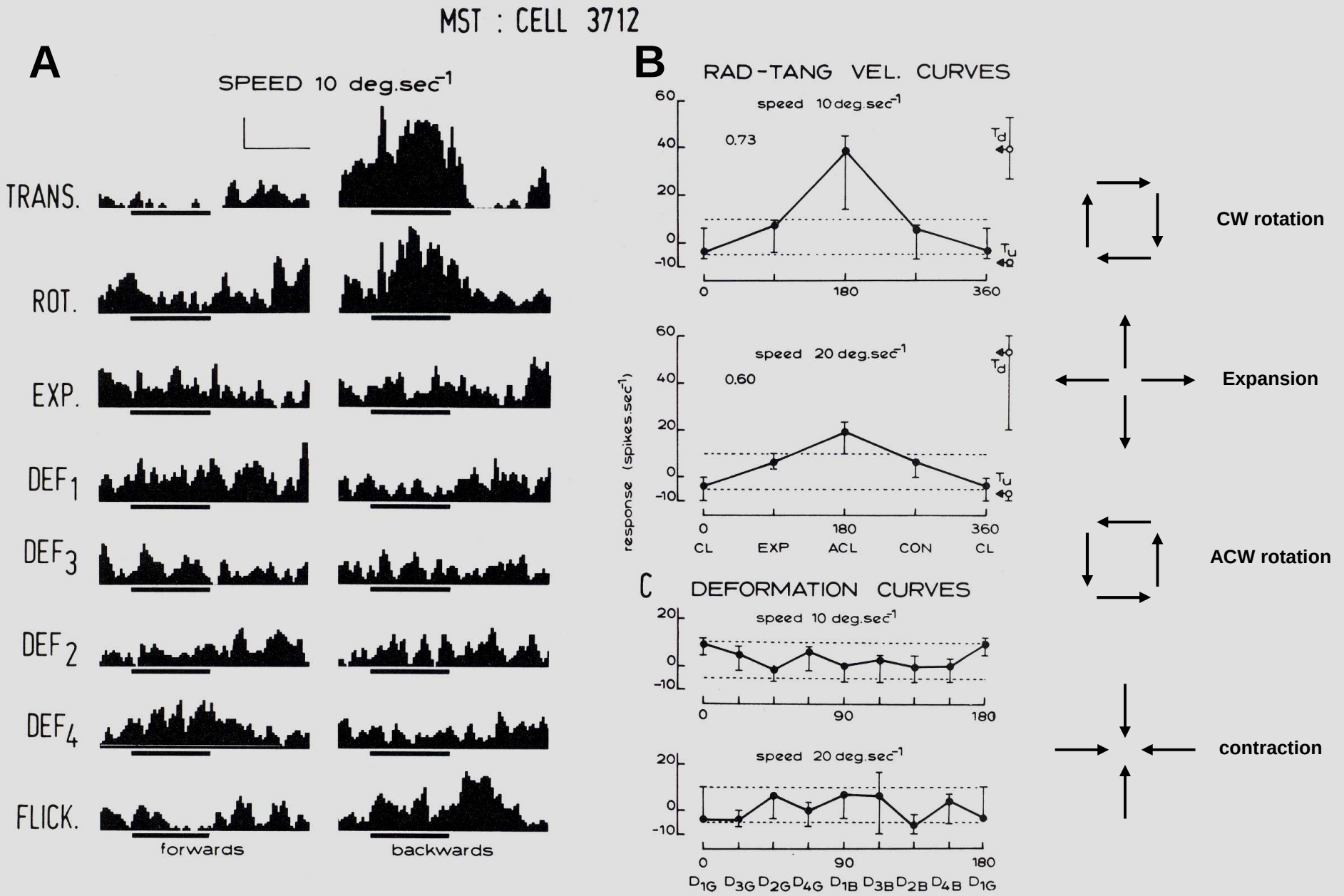

L. Lagae et al, J. of Neurophys., ´94

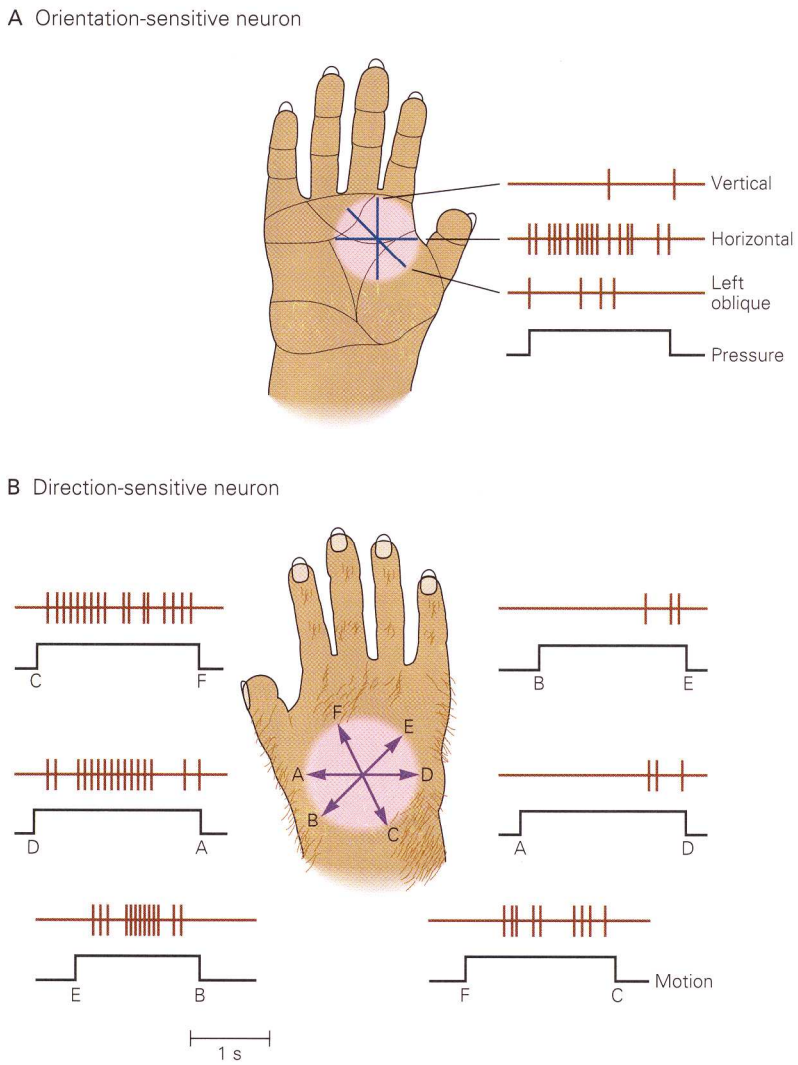

Figure 23-13 **Feature-detection neurons in area 2 of the primary somatic sensory cortex respond to highly specific features of a stimulus.** The examples shown here are from a macaque monkey.

A. This orientation-sensitive neuron distinguishes horizontal and vertical edges pressed on the palm. The neuron responds vigorously when the edge is oriented horizontally but is nearly silent when the edge is oriented vertically. Responses to the oblique orientation are weaker than those to the horizontal position. (Adapted from Hyvärinen and Poranen 1978.)

B. This direction-sensitive neuron responds most vigorously to movement across the hand toward the thumb and index finger. The neuron displays its strongest responses to motion in the radial direction (D to A and E to B); the weakest responses occur in the ulnar direction (A to D and B to E). Responses to distal movements toward the fingers (C to F) are more vigorous than responses to proximal movements toward the wrist (F to C). The trace below each cell record shows the duration of motion and the start and end points of the path. (Adapted from Costanzo and Gardner 1980.)

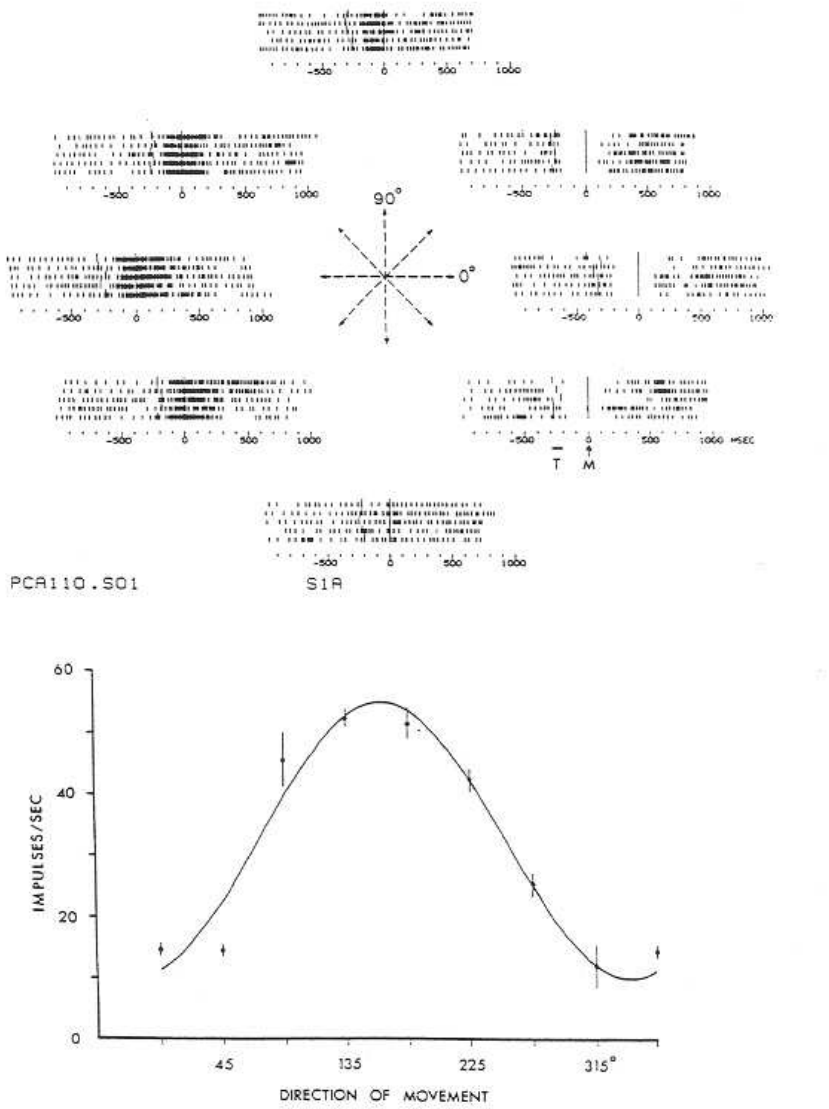

Figuur 11.12 – Orderly variation in the frequency of discharge of a motor cortical cell with the direction of movement. *Upper half*, Rasters are oriented to the movement onset, *M*, and show impulse activity during five repetitions of movements made in each of the eight directions indicated by the *center diagram*. Notice the orderly variation in cell's activity during the RT, MT and TET. *Lower half*, Directional tuning curve of the same cell. The discharge frequency is for TET. The data points are the mean ± SEM. The regression equation for the fitted sinusoidal curve is $D = 32.37 + 7.281 \sin \theta - 21.343 \cos \theta$, where D is the frequency of discharge and θ is the direction of movement or, equivalently, $D = 32.37 + 22.5 \cos (\theta - \theta_0)$, where θ_0 is the preferred direction ($\theta_0 = 161°$).

Fig 03

AIRE CORTICALE

SYSTEME CEREBRAL

Critères de Définition des Aires Corticales

- 1) Cyto- et Myeloarchitectonie
- 2) Connections avec aires
- 3) Organisation topographique
- 4) Propriétés neuronales

Cortex visuel primaire (dans la calcarine)

- 1) couche 4 epaisse (aire 17); blobs cytochrome oxydase en couches 2-3
- 2) afferences du genouille lateral
- 3) retinotopie precise et complete (V1)
- 4) neurones monoculaires et cellules simples

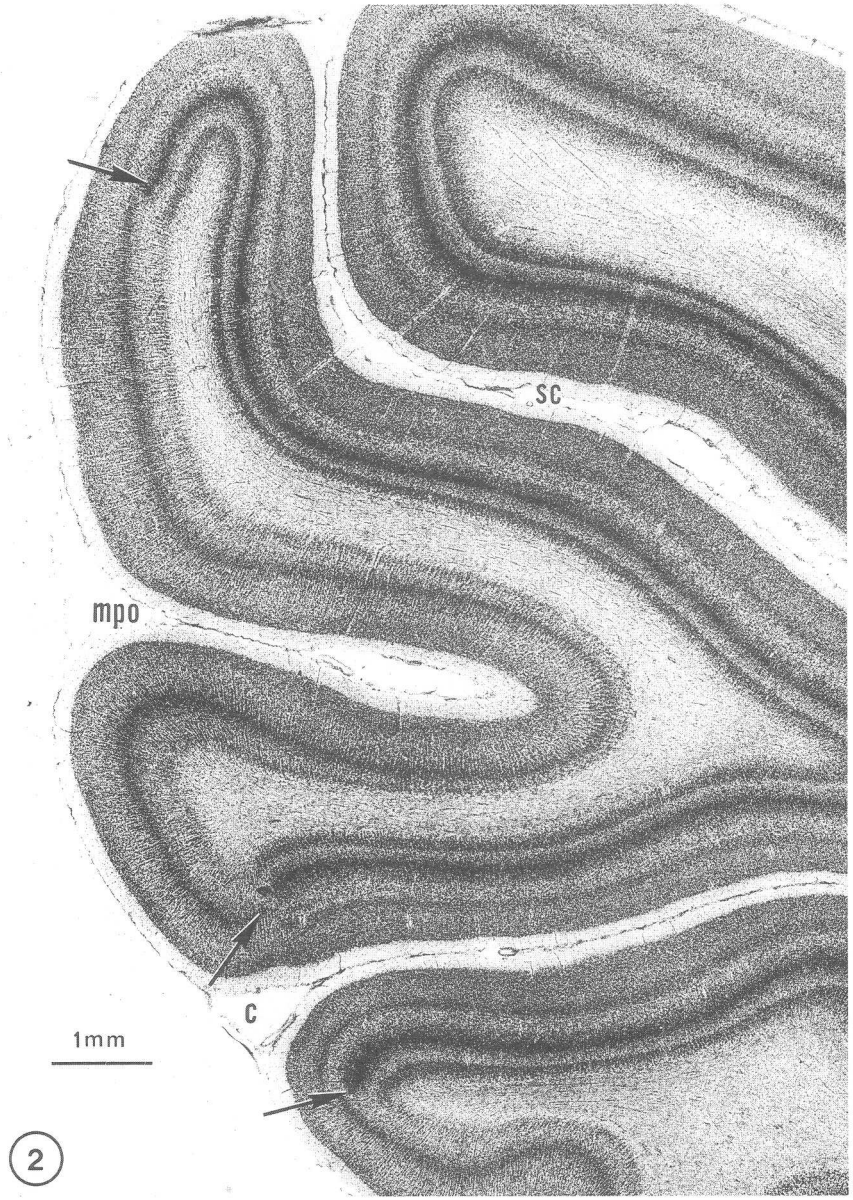

Figure 2. A Nissl-stained coronal section through the occipital pole of the macaque cerebral hemisphere. The medial surface of the hemisphere, on the left, is occupied by area 18 (V2), and at this level it is indented by the medial parieto-occipital sulcus (mpo). Below, area 17 starts (arrows) at the lips of the calcarine fissure (c), where the dark layer IV of area 18 splits to form the complex layer IV of primary visual cortex. Another transition between areas 18 and 17 is also apparent just below the superior ramus of the calcarine fissure (sc).

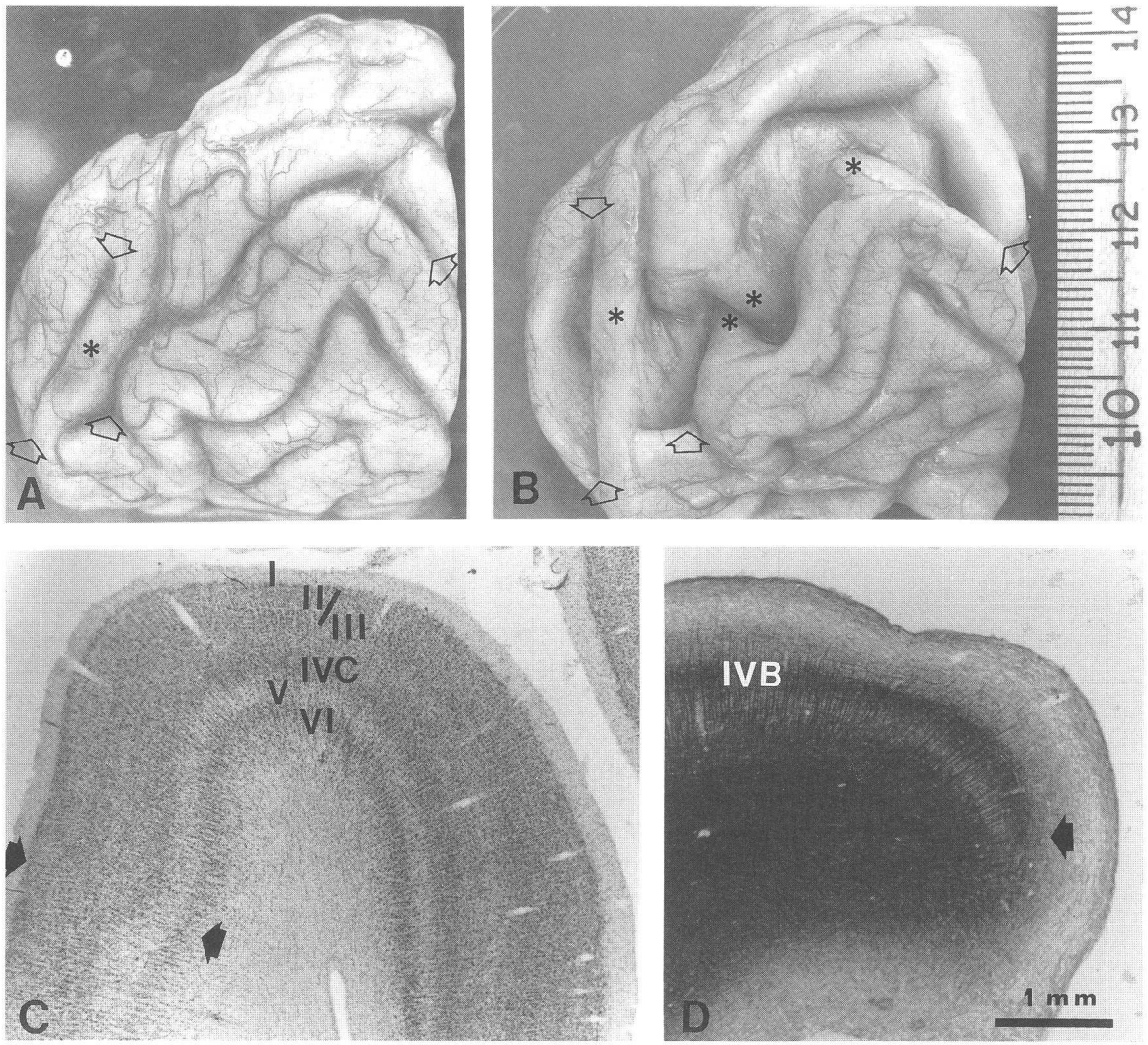

Figure 1. (A, B) Photomacrographs of the medial aspect of the left occipital lobe from a 72-year-old man. (A) Undisturbed specimen, showing the curved pattern of the calcarine fissure (ends marked with hollow arrows), which is interrupted by a cuneolingual gyrus (asterisk). (B) After opening part of the calcarine fissure, its complex pattern of folding can be appreciated. This contains about two-thirds of the primary visual cortex. Three additional small cuneolingual gyri can be appreciated within the calcarine fissure (asterisks), in addition to the more posterior cuneolingual gyrus that was visible in the interhemispheric fissure prior to dissection (asterisk in A), (C, D) Photomicrographs of cresyl violet and myelin (Gallyas) stains, respectively, cut perpendicularly to the lip of the calcarine fissure. They illustrate low-power views of the striking laminar organization of the striate cortex, and especially its distinctive layer IV, which can be easily seen to end abruptly at the boundary with the prestriate cortex (area 18 of Brodmann, 1903), indicated by the solid arrows. Roman numerals designate cortical layers described in detail in the text.

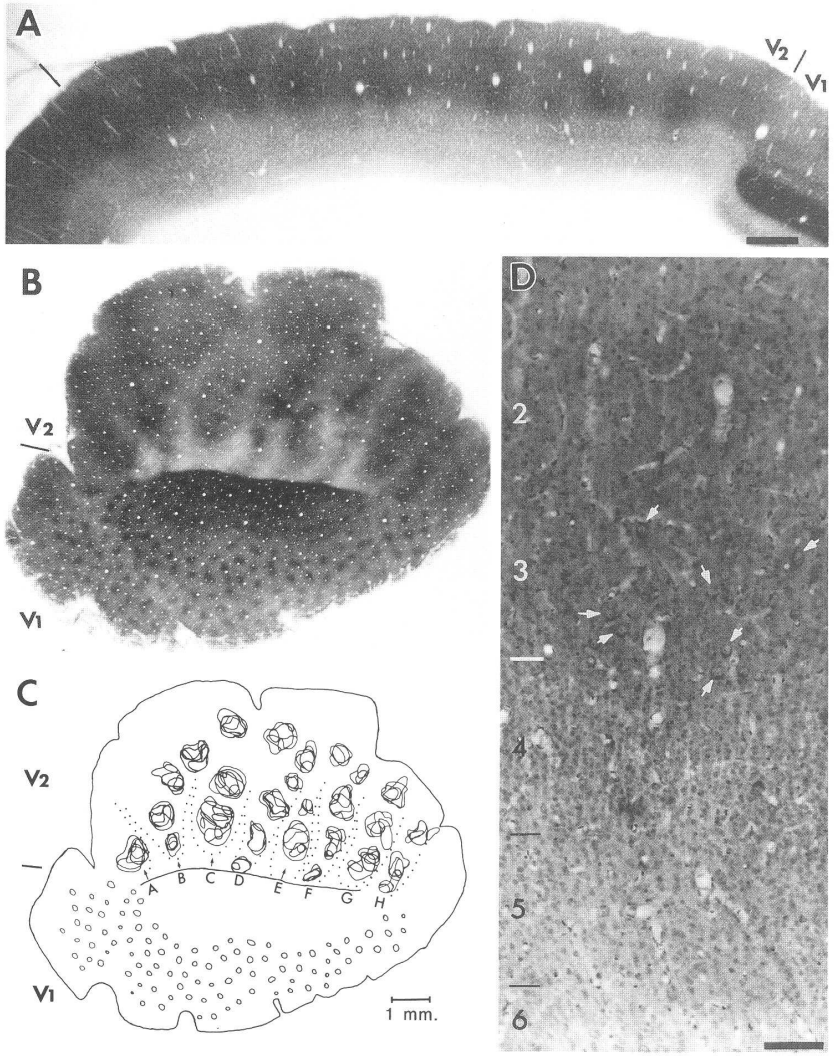

Figure 14. V2 of the squirrel monkey reacted for CO. (A) Cross section of the V1/V2 border showing the abrupt transition of CO pattern. In V2, periodic zones or puffs of high CO activity appear in layers 2 and 3, extending into the upper edge of 4. There is a hint of a columnar pattern of staining, with layers 4 and 5 below the puffs being slightly more reactive than the adjacent region. A thin band of staining can also be seen in upper 5 (5A) and another one between 5 and 6. The black lines above the section demarcate the approximate boundaries of V2 where distinct supragranular puffs can be seen in periodic array. (B) Tangential section showing the small and closely spaced puffs in V1 and larger puffs forming thick and thin stripes in V2. (C) Camera lucida tracing of puffs in V2 through seven tangential sections spaced 120 μm apart. Note that the puffs remain globular with some irregular boundaries, and that they form alternating wide (A, C, E, G) and narrow (B, D, F, H) stripes. The puffs in the thin stripes tend to be smaller and begin right at the V1/V2 border. (D) CO-reacted and Nissl-counterstained coronal section through V2, showing the location of the puff

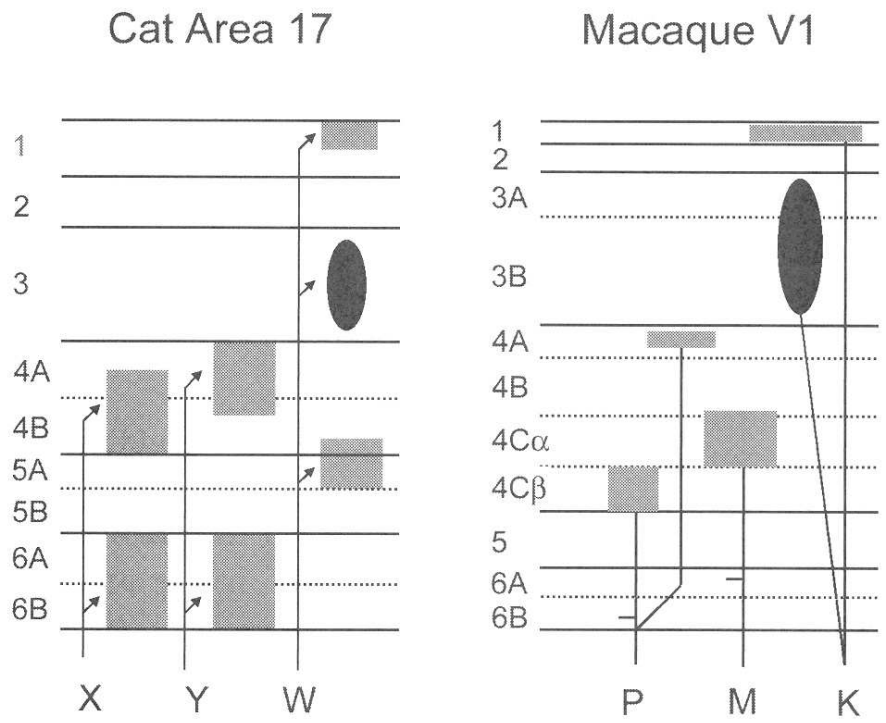

FIGURE 31.1 LGN projection patterns to visual cortex of cats and macaque monkeys. *Left*: projections from the LGN to V1 in the cat. X and Y LGN cells send axons to layers 4 and 6. W cells project CO blobs in layer 3 and to layers 1 and 5a. *Right*: projections from the LGN to V1 in macaque monkey. M and P cells project, respectively, to layers 4Cα and 4Cβ while K cells project to the CO blobs in layer 3 and to layer 1. In addition, P cells have been proposed to send axons to layer 4A. LGN projections to layer 4A are missing in apes, humans, and some other primates. Some M and a few P cells have collateral branches terminating sparsely in layer 6. See text for details. (*Left*: Data from Boyd and Matsubara, 1996; Humphrey et al., 1985; Kawano, 1998; *Right*: modified from Casagrande and Kaas, 1994, with permission of the publisher.)

V. A. Casagrande and X. Xu

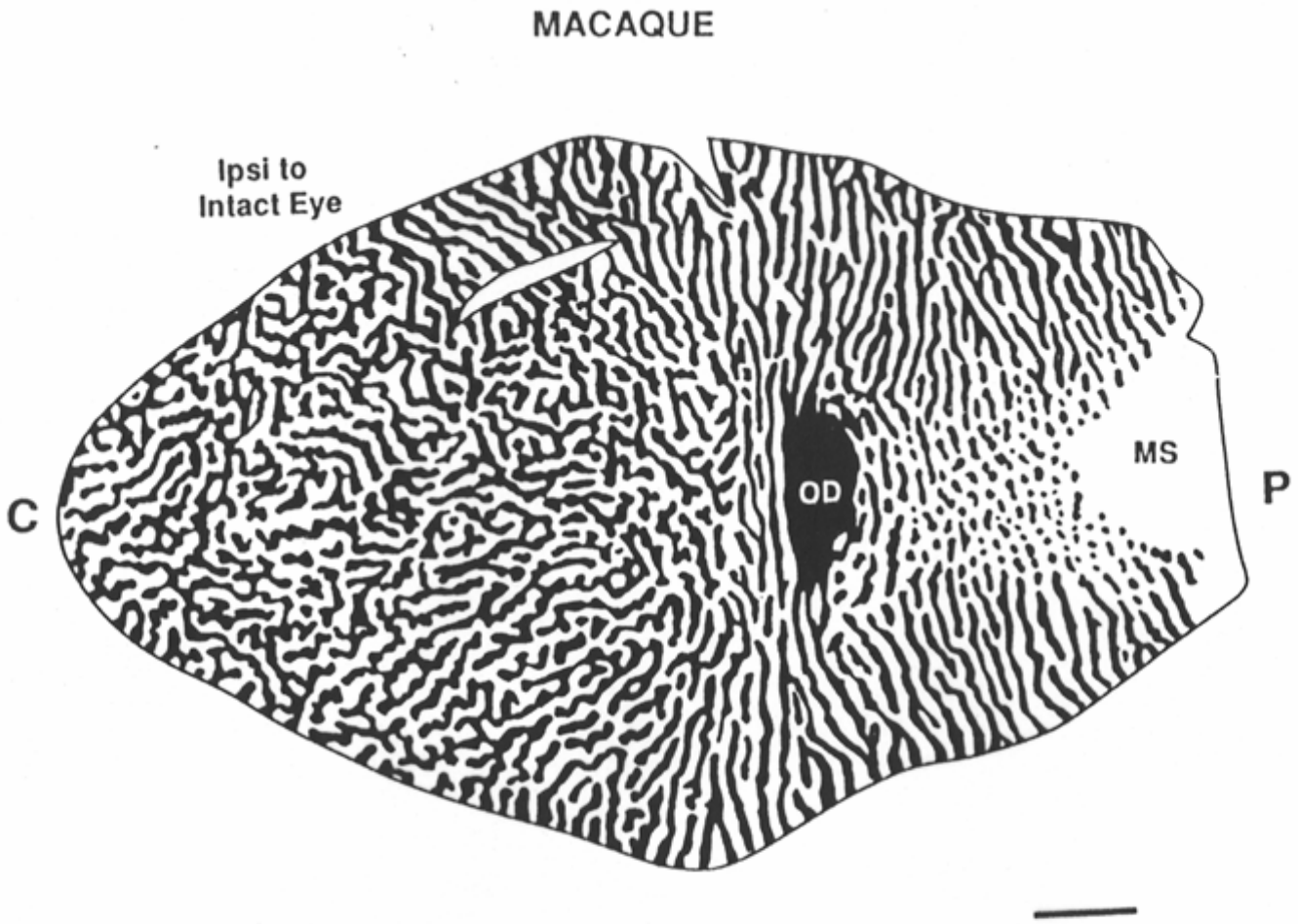

Figure 5. The complete pattern of ocular dominance bands in area 17 of a macaque monkey (*Macaca fascicularis*). The dark cytochrome oxidase regions relate to the intact ipsilateral eye (black) and light CO regions (white) relate to the suppressed contralateral eye. The figure is based on a complete reconstruction of area 17 from artifically flattened cortex cut parallel to the surface. The black oval corresponds to the projection of ipsilateral retina matched by the retina-free optic disk in the contralateral eye. The large, white area on the right corresponds to the monocular field with input only from suppressed contralateral eye. Central vision is on the left. Bar = 1 mm. Modified from Florence and Kaas (1992) with permission.

Florence and Kaas, ´92

Topografische organisatie

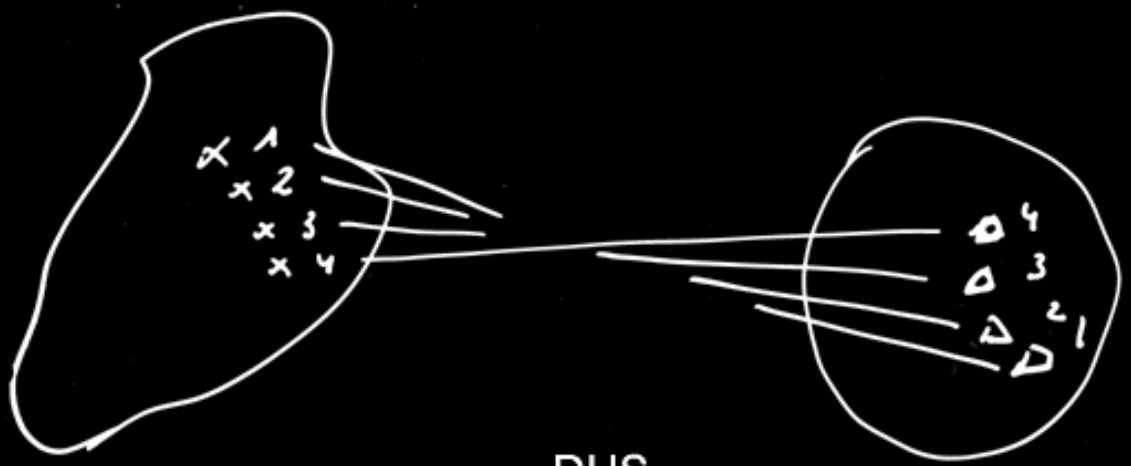

DUS

naburige neuronen hebben naburige R.V.

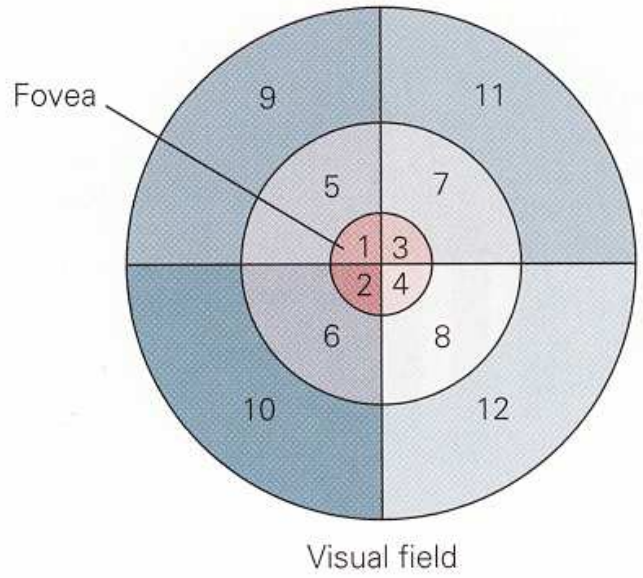

Figure 27-9 Each half of the visual field is represented in the contralateral primary visual cortex. In humans the primary visual cortex is located at the posterior pole of the cerebral hemisphere and lies almost exclusively on the medial surface. (In some individuals it is shifted so that part of it extends onto the lateral surface.) Areas in the primary visual cortex are devoted to specific parts of the visual field, as indicated by the corresponding numbers. The upper fields are mapped below the calcarine fissure, and the lower fields above it. The striking aspect of this map is that about half of the neural mass is devoted to representation of the fovea and the region just around it. This area has the greatest visual acuity.

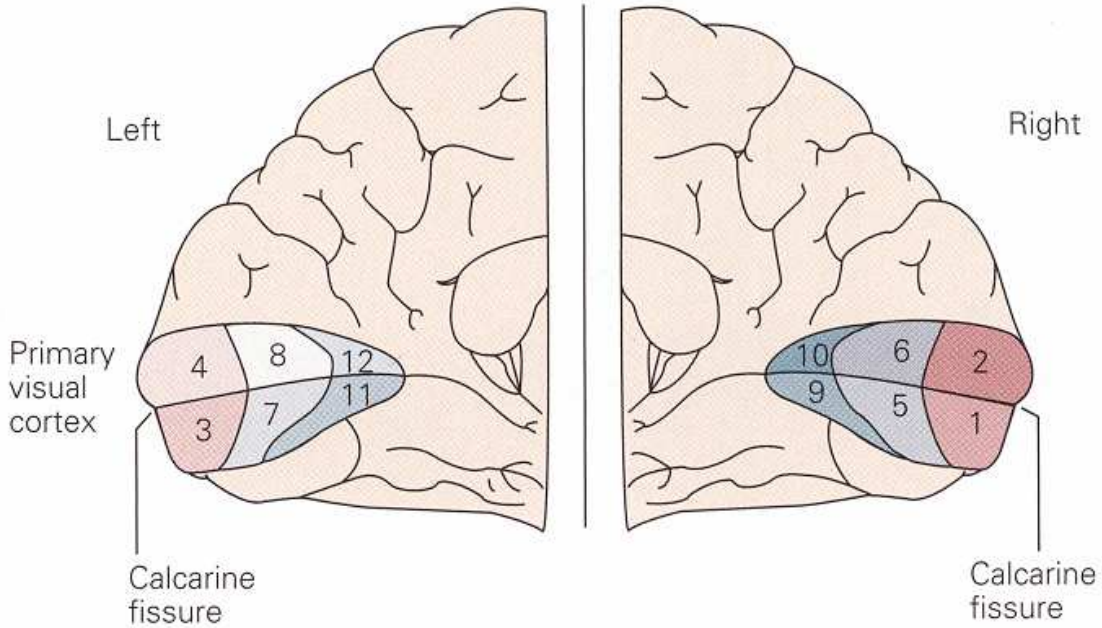

Eric R. Kandel et al

Aire MT/V5 (dans sillon temporal superieur)

- 1) myelinisation forte
- 2) afferences de V1
- 3) retinotopie plus grossiere avec hemichamp complet
- 4) selectivite pour la direction de mouvement pour la vaste majorite des neurones

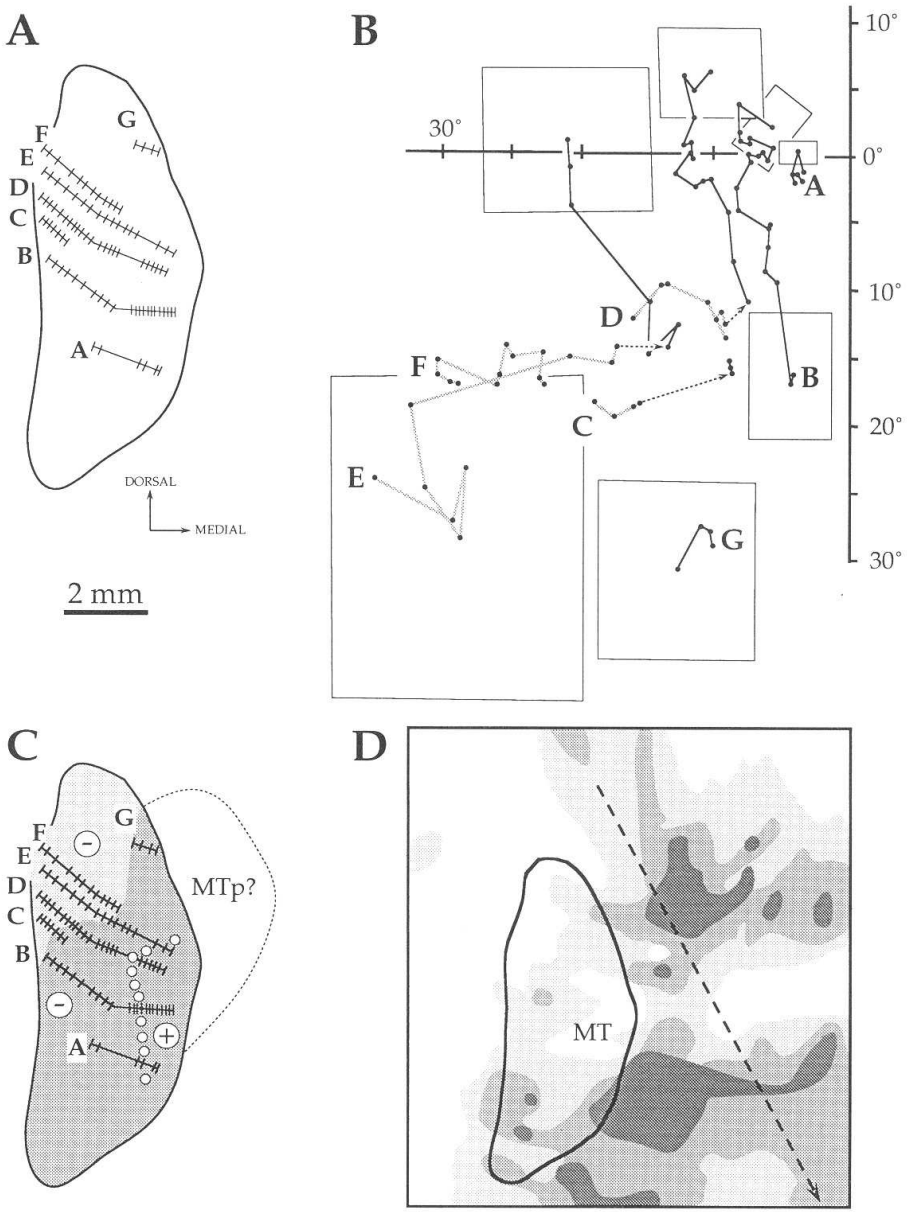

Figure 7. Topographic organization of visual area MT in the macaque. Recording sites (A) and receptive fields (B) in macaque area MT, redrawn from Fig. 3 of Maunsell and Van Essen (1987). (A) An unfolded reconstruction of the caudal bank of the superior temporal sulcus, with the myeloarchitectonic boundaries of area MT indicated. Seven sequences of recording sites, labeled A–G from ventral to dorsal, are indicated (ticks indicate the location of individual recording sites). (B) The location of corresponding receptive field centers and selected receptive field borders in the contralateral hemifield. The visuotopic organization of MT in the macaque appears to be much more complex than in New World monkeys. For example, the representation of the lower quadrant is many times larger than that of the upper quadrant, and the neurons with receptive fields nearest to the vertical meridian in some sequences (e.g., D, E) are found far from the border of MT. (C) Reanalysis of the same data with the visual field sign criterion, which distinguishes MT from surrounding areas in New World monkeys (Sereno *et al.*, 1994). The sector of mirror-image representation is shaded light gray, and the sector of non-mirror-image representation dark gray. If MT is defined as the sector of non-mirror-image representation, a simple and relatively more ordered first-order representation is observed in this area. The dotted line to the right of MT indicates an estimate of MTp, or the sector of peripheral representation in MT (Ungerleider and Desimone, 1986). Similar to MT, MTp receives direct projections from V1, but it is less densely myelinated. (D) Pattern of callosal connections in the same animal, redrawn from Fig. 11 of Maunsell and Van Essen (1987). In this bidimensional reconstruction, the dashed line indicates the fundus of the superior temporal sulcus, the continuous line the myeloarchitectural borders of MT, and the gray fill the pattern of interhemispheric connections of MT and surrounding areas, as evaluated with the Wiitanen (1969) method. Dark gray indicates dense degeneration, intermediate gray moderate degeneration, and light gray sparse degeneration. A callosal-free ring is observed within MT, similar to New World monkeys (Newsome and Allman, 1980).

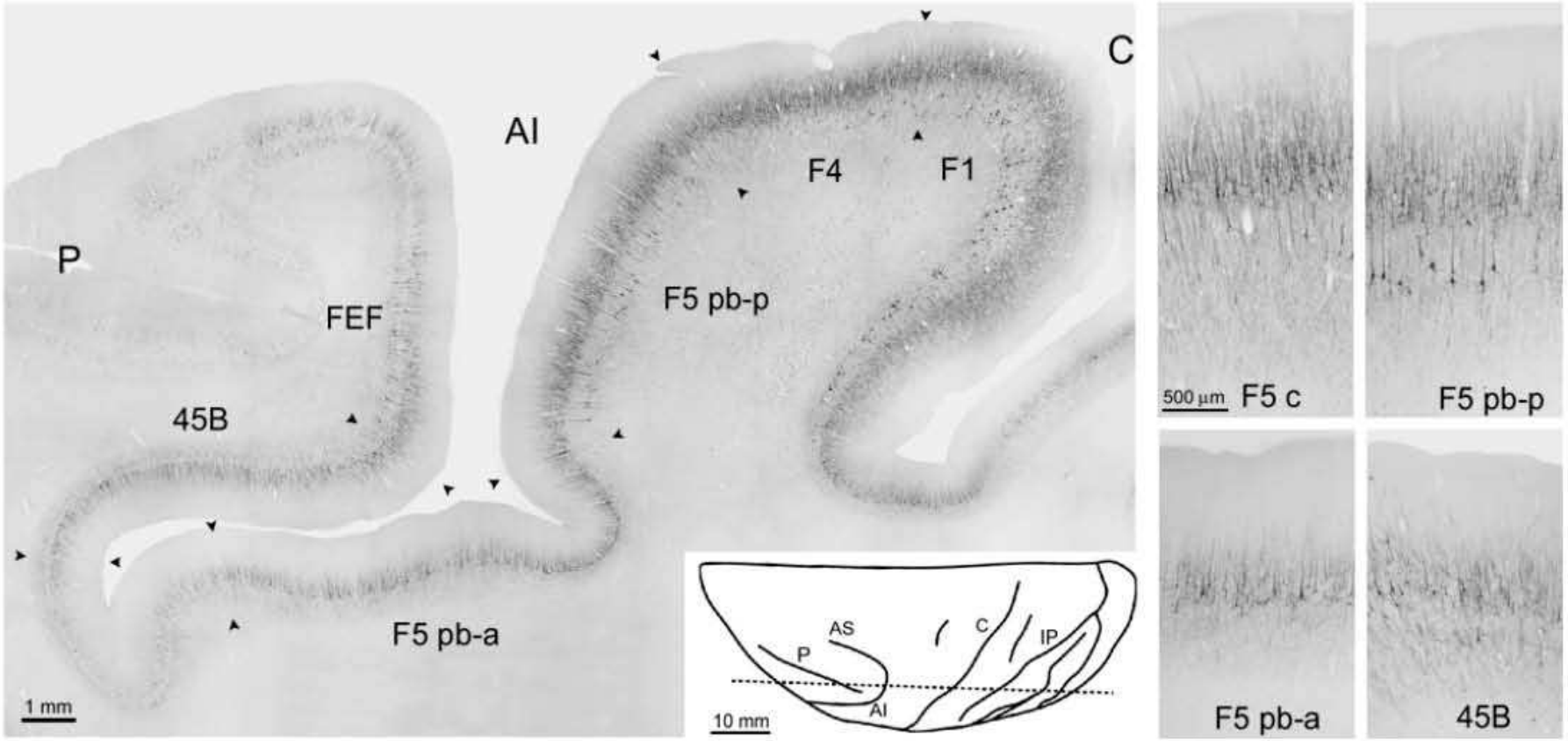
P
FEF
45B
AI
F4
F1
C
F5 pb-p
F5 pb-a
1 mm
AS
P
AI
C
IP
10 mm
500 µm
F5 c
F5 pb-p
F5 pb-a
45B

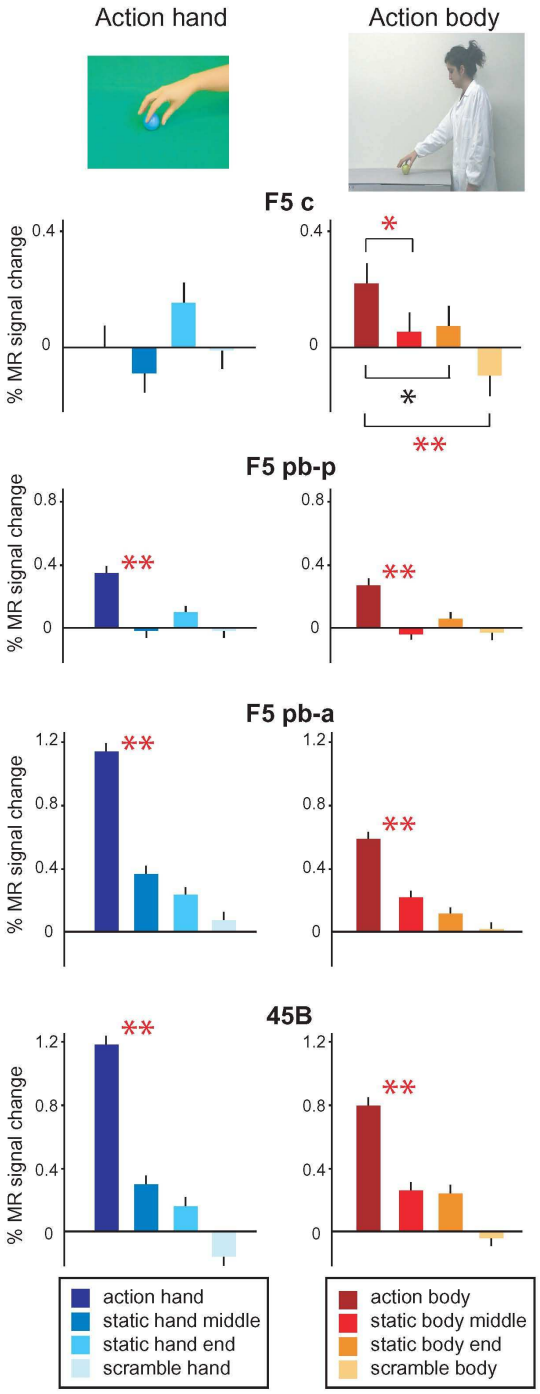
Action hand
Action body
F5 c
F5 pb-p
F5 pb-a
45B
% MR signal change
0.4
0
0.8
1.2
*
**
action hand
static hand middle
static hand end
scramble hand
action body
static body middle
static body end
scramble body

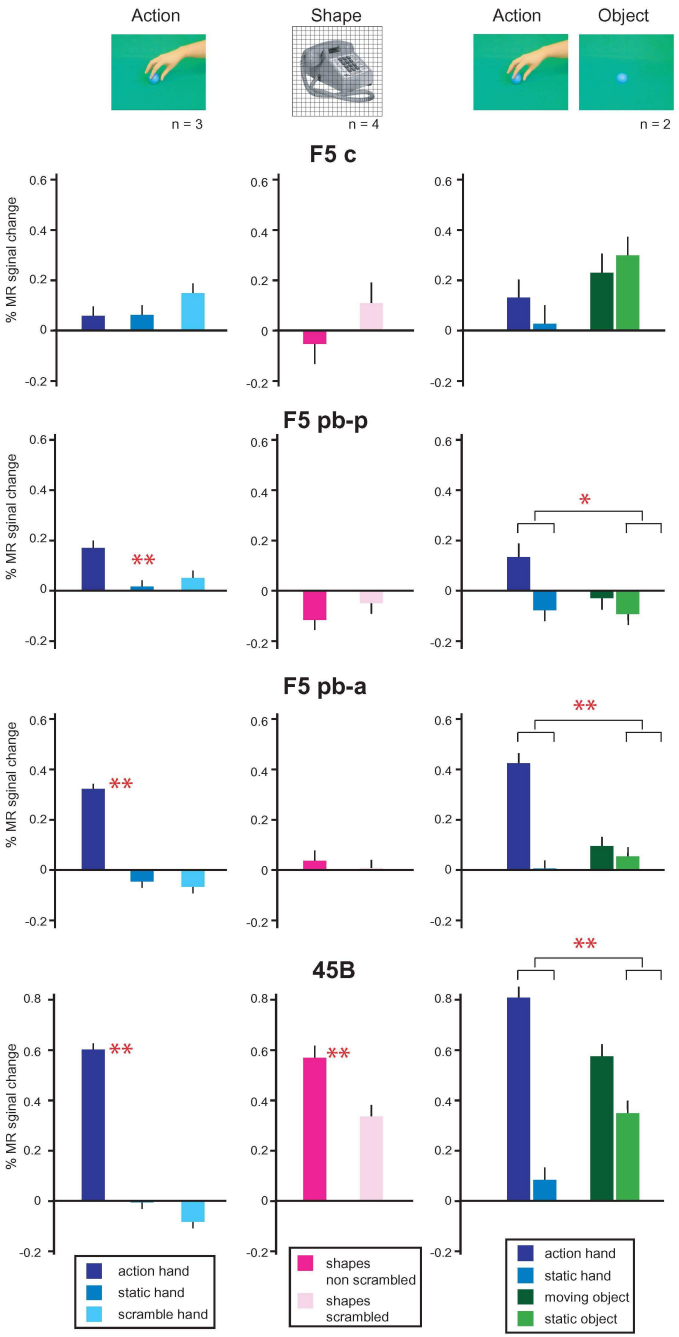
Action
Shape
Action
Object
n = 3
n = 4
n = 2
F5 c
F5 pb-p
F5 pb-a
45B
% MR signal change
0.6
0.4
0.2
0
-0.2
0.8
**
*
action hand
static hand
scramble hand
shapes
non scrambled
shapes
scrambled
action hand
static hand
moving object
static object

1) Connections et hierarchie (singe)

Types de connections

- Projections en avant
- projections en retour
- projections laterales
- projections locales

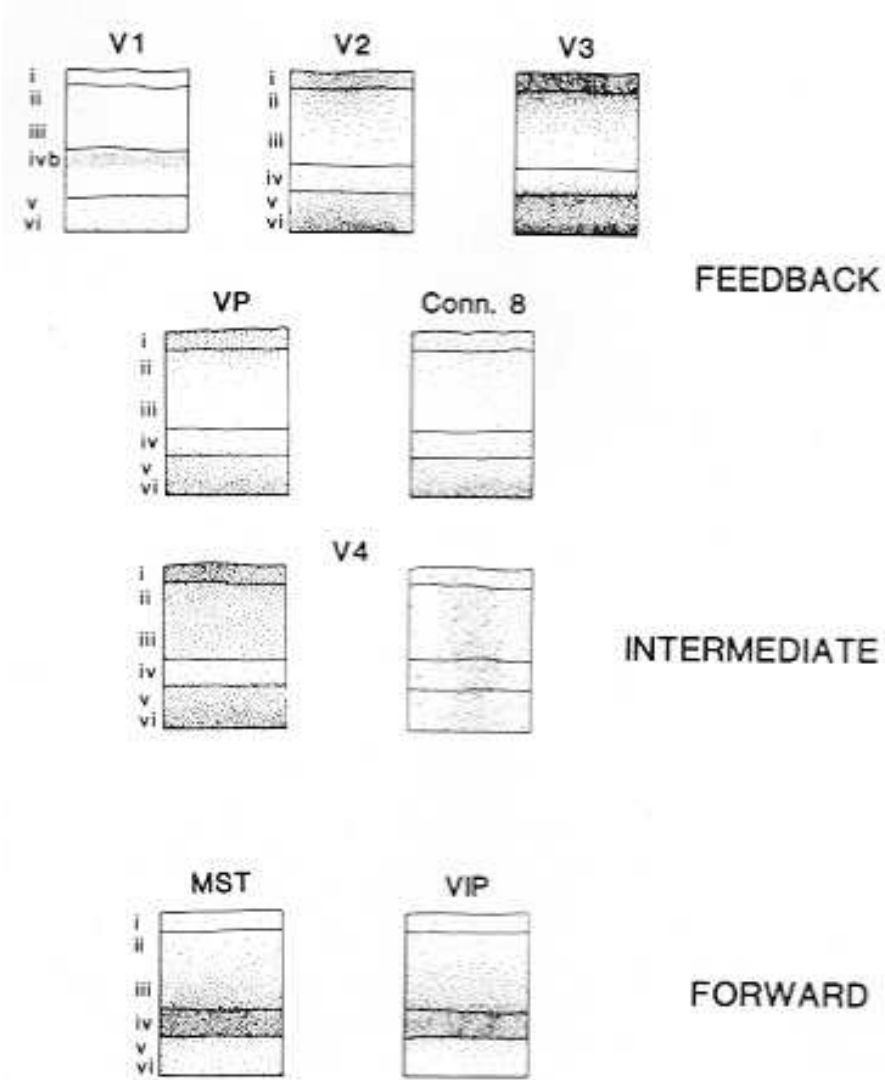

The laminar distribution of anterogradely transported label after MT injections. The laminar distribution of label is shown for each cortical target of MT. Feedback projections from MT are characterized by terminating largely in layers I and VI and sparing layer IV. Forward projections terminate mainly in layers IV and III. Two different laminar distributions were found in V4, one sparing layer IV and the other labeling all layers about equally (see the text). From Maunsell and Van Essen (1983c).

Mausell and Van Essen, ´83

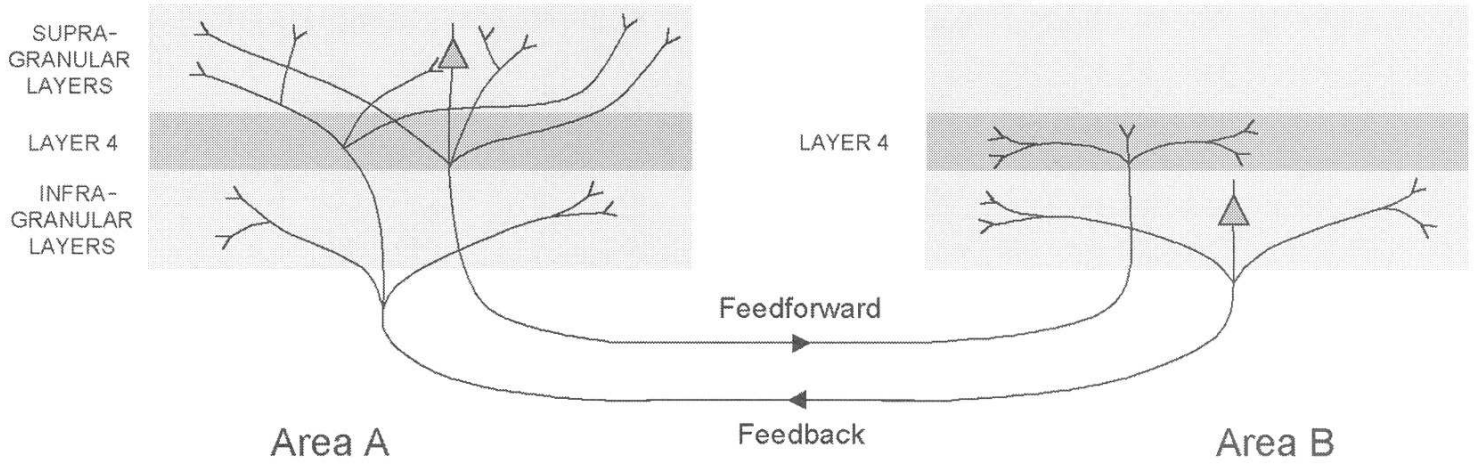

FIGURE 33.1. Schematic representation of the laminar distributions of feedforward and feedback neurons and axonal terminal arborizations. Note the presence of axon collaterals that innervate neighboring neurons and constitute the majority of horizontal connections.

J. Bullier

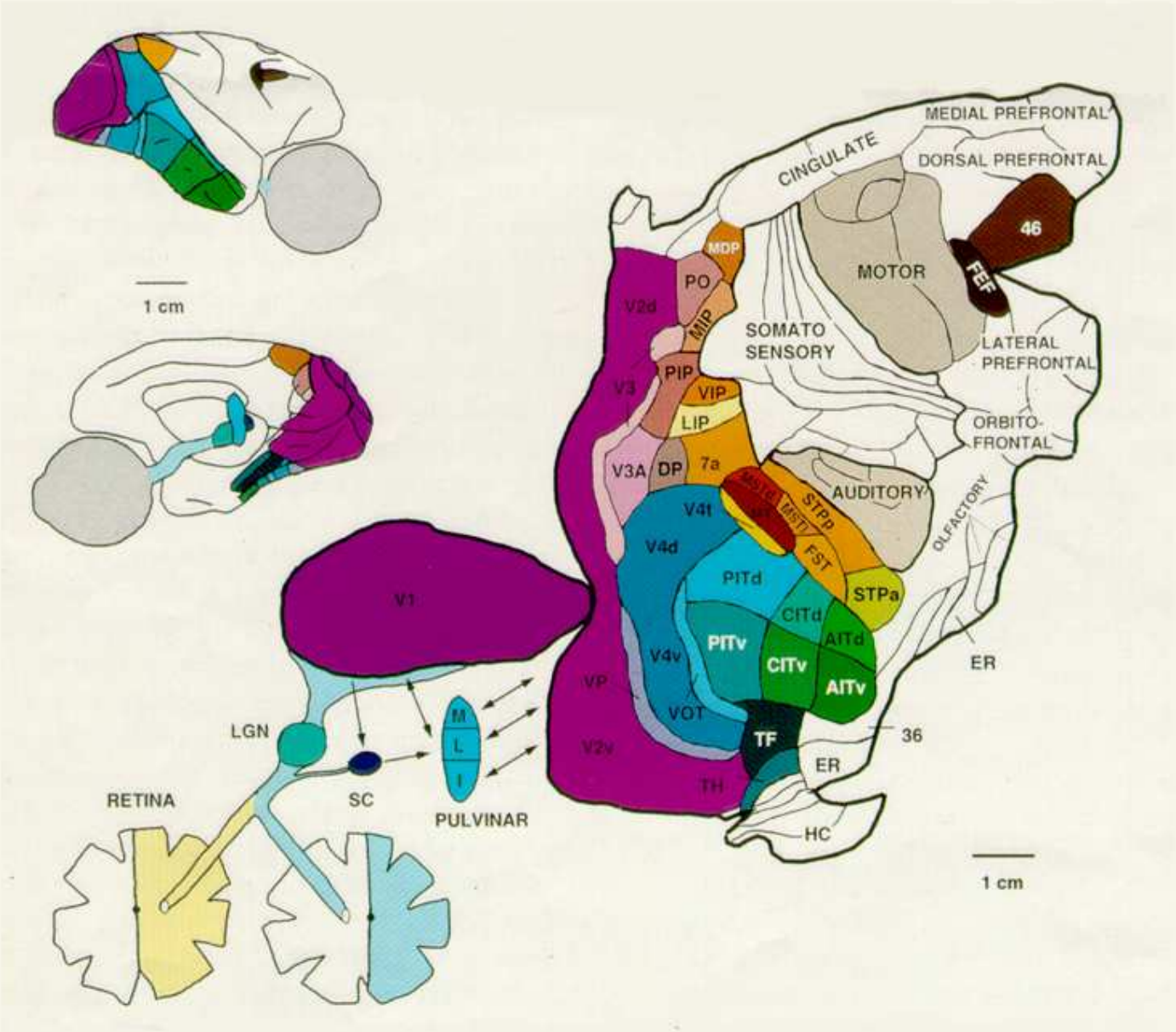

David C.Van Essen, et al., ‘92

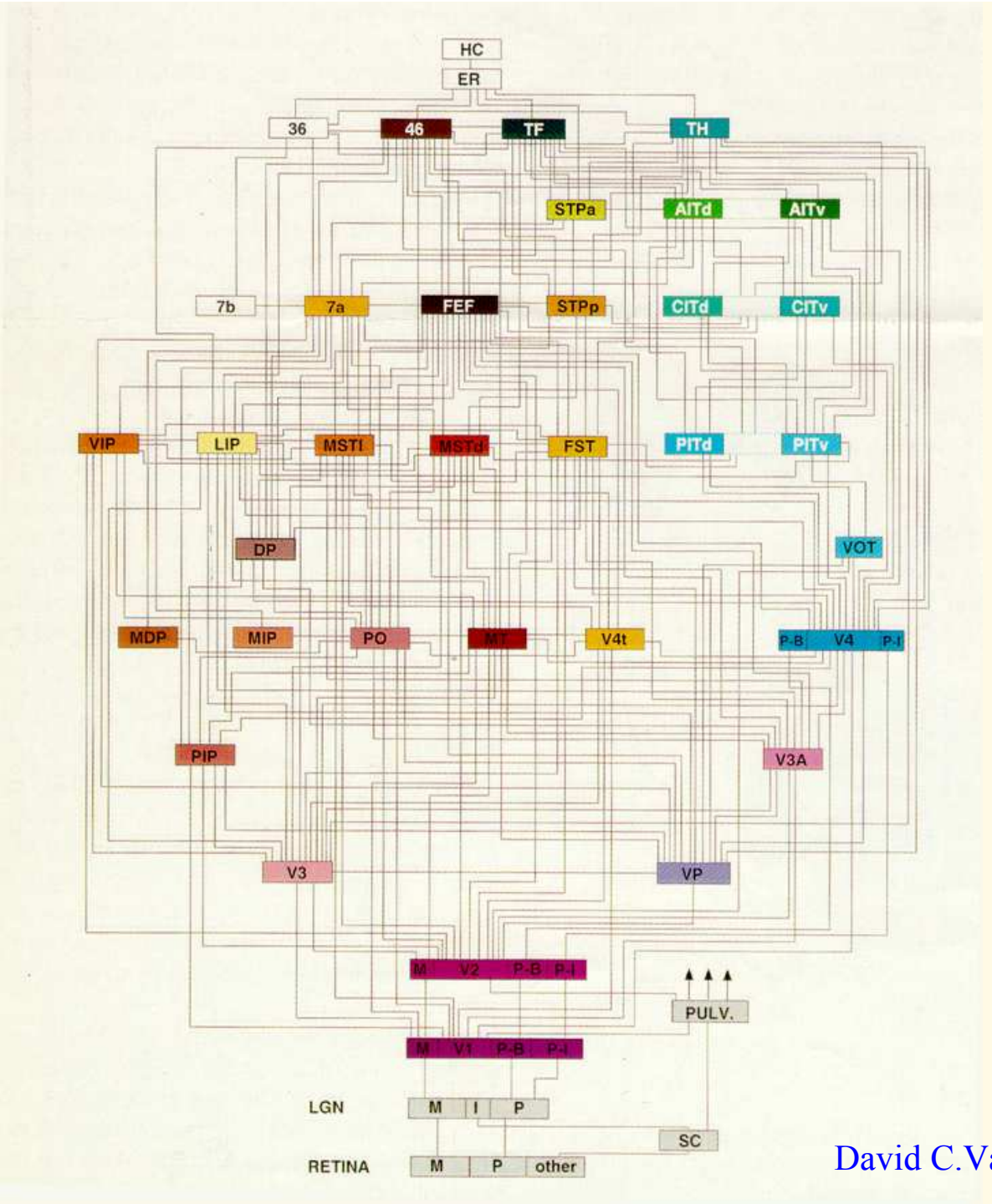

David C.Van Essen, et al., ‘92

Critères de Définition des Aires Corticales Humaines

- Cyto- et Myeloarchitectonie ??
- Connections (avec aire connue) ??
- 1) Organisation topographique (IRMf)
- 2) Propriétés fonctionnelles (IRMf)
- 3) Localisation géographique (par rapport aux aires connues)

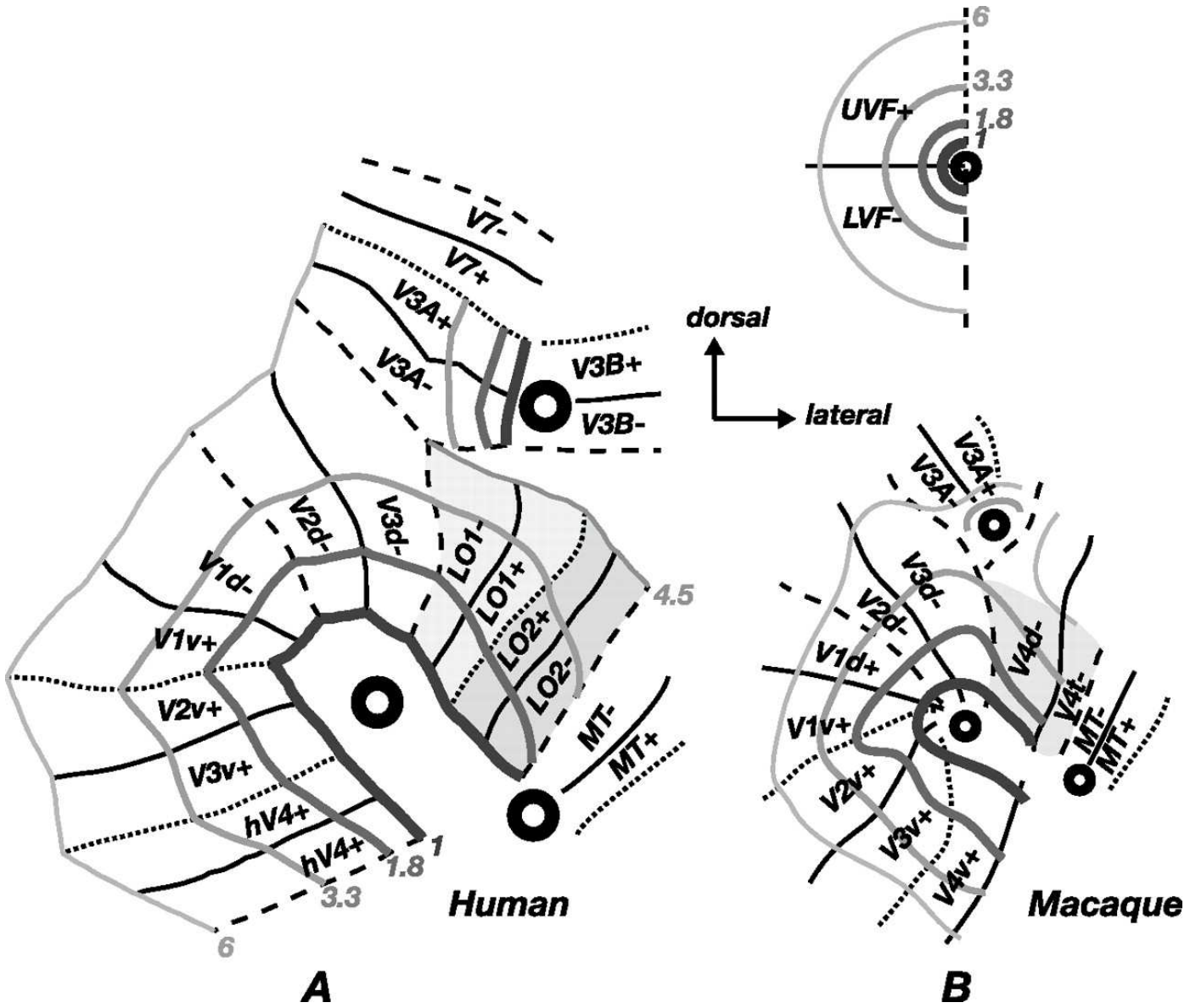

Schematic summary of visual field topography. ***A***, Human visual cortex. Topography and location of LO1 and LO2 relative to other retinotopic visual areas (shown in flattened format for the right hemisphere) averaged across all 30 hemispheres (for details of intersubject averaging, see Materials and Methods). ***B***, The organization of the corresponding region of macaque visual cortex is shown for comparison (not to scale). Adapted from Gattass et al. (1988), Brewer et al. (2002), and Fize et al. (2003). UVF, Upper visual field; LVF, lower visual field.

J. Larsson and D.J. Heeger JONS 2006